Tailoring the Electrocaloric Effect by Internal Bias Fields and Field Protocols

Yang-Bin Ma,[1] Bai-Xiang Xu,[1,*] Karsten Albe,[1] and Anna Grünebohm[2]

[1] *Institute of Materials Science, Technical University of Darmstadt, 64287 Darmstadt, Germany*

[2] *Faculty of Physics and Center for Nanointegration (CENIDE), University of Duisburg-Essen, 47048 Duisburg, Germany*

(Received 14 May 2018; revised manuscript received 10 July 2018; published 30 August 2018)

Defect dipoles, strain gradients, and the electric boundary conditions at interfaces and surfaces often impose internal bias fields in acceptor-doped ferroelectrics, ferroelectric films, nanocomposites, and multilayers. In this work, we study the impact of internal bias fields on the electrocaloric effect (ECE), utilizing an analytical model and *ab-initio*-based molecular-dynamics simulations. We reveal the complex dependency of the ECE on field protocol and the relative strength of internal and external fields. The internal fields may even reverse the sign of the response (inverse or negative ECE). We explore the transition between conventional and inverse ECE and discuss reversible and irreversible contributions to the field-induced specific entropy change. Most importantly, we predict design routes to optimize the cooling and heating response for small external fields by the combination of internal field strengths and the field-loading protocol.

DOI: 10.1103/PhysRevApplied.10.024048

I. INTRODUCTION

The electrocaloric effect (ECE) in ferroelectrics is promising for solid-state cooling devices [1,2] as an external electric field can induce large changes of specific entropy (ΔS) with respect to temperature (ΔT). Commonly, an external field reduces the specific dipolar entropy and the material heats up under the application of a field adiabatically (conventional or positive ECE). In some cases, adiabatic cooling under the application of a field has also been found (inverse or negative ECE) [3–9]. The inverse ECE might have the potential to enhance the overall caloric response and attracts considerable research interest, as reviewed in Refs. [10–12].

One prominent way to optimize ferroelectric properties is acceptor doping, i.e., substitution with ions of lower valence. In this case, charge neutrality is achieved by oxygen vacancies. For example, Ti ions in $BaTiO_3$ can be substituted with Mn, Cu, or Fe ions. Over time, the dopants and oxygen vacancies form associated defect dipoles [13]. As shown experimentally, these dipoles can be unidirectionally aligned, for example, by a long-time poling process [14,15]. Due to the high activation barrier for oxygen vacancy migration, these defect dipoles are almost nonswitchable in the ferroelectric phase around room temperature on time scales that are relevant for cooling devices [16,17]. There are numerous studies dealing with the influence of defect dipoles on material properties (see the review article in Ref. [18]). In particular, Han *et al.* [19] observed that defect dipoles induce an internal electrical field which can shift the hysteresis (see Fig. 1). The occurrence and direction of the shift depend on the alignment of the defect dipoles and thus on the previous field and heat treatment of the material. Large modifications of the functional responses by such doping are possible [16,20].

So far, only a few studies have explored the impact of acceptor doping on the ECE. It has been reported that co-doping with Mn and Y modifies the ECE in $Ba_{0.67}Sr_{0.33}TiO_3$ [21], and our previous studies on doped $BaTiO_3$ have revealed the possibility of shifting the ΔT-peak to higher temperatures [22,23]. Remarkably, we found an inverse ECE in the presence of defect dipoles aligned antiparallel to the external field and a transition between inverse and conventional ECE with the strength of the external field [22,23]. In addition, we found that the ECE for field application may exceed the ECE for field removal [23], and that the response for different initial states (prepared by either field cooling or field heating) may differ by one order of magnitude in certain temperature intervals [22].

Analogously, internal bias fields are commonly observed in nanocomposites, ferroelectric films, and multilayers [24–30]. These bias fields have been related to heterostructure [29,30], stress gradients [26], asymmetric electric boundary conditions [27], and ferroelectric blends in a relaxor matrix. Qian *et al.* [24,25] reported that the ECE in a relaxor ferroelectric polymer can be enhanced by

*xu@mfm.tu-darmstadt.de

 © 2018 American Physical Society

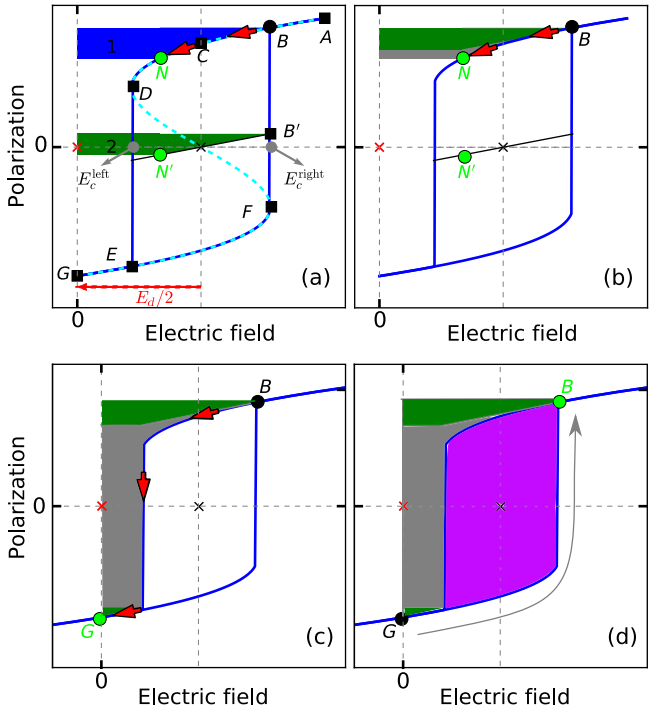

FIG. 1. A schematic of a $P(E_{ex})$ loop in the presence of an internal field E_d. Several characteristic points can be defined: E_c^{left} and E_c^{right}, coercive fields; B and E, the boundaries of the hysteretic region; D and F, inflection points. (a),(b) For a field change from E_B to E_N, the areas corresponding to reversible and actual work densities $|W_r|$ and $|W_{\text{actual}}|$ are colored in green and blue, respectively. The superposition of both areas yields the work loss $|W_{\text{loss}}| = |W_{\text{actual}} - W_r|$, colored in gray. Note that W_{loss} is negative for the field protocol used, in contrast to the positive W_{loss} for $C \rightarrow N$ without internal fields [37]. (c) For the full removal of E_{ex}, the same as (b) with the gray area showing the work losses: the positive E_c^{left} induced by the internal field allows for large negative work losses. (d) For field application, W_{loss} is positive and exceeds the negative loss for field removal by the area of the hysteresis (pink).

45% when ferroelectric polymer blends are introduced, inducing internal bias fields [24,25]. Similar to our findings for defects, they found inverse ECE in the presence of internal bias fields as well. Therefore, it is important to obtain a detailed understanding of the impact of internal bias fields on the ECE, and tap the full potential of the bias fields.

In the literature, the ECE is mostly determined indirectly [8,21,31–35]. However, there are several limitations of the indirect approach, as reviewed in Ref. [36]. In particular, irreversible specific entropy contributions related to ferroelectric switching or first-order phase transitions are commonly not taken into account [12,37]. Alternatively, ΔT can be measured or simulated directly [23,38–46]. So far, direct temperature changes have been mainly determined for a unipolar field loading (field application or removal for one field direction) and the possible impacts of thermal and field hysteresis have been widely neglected. However, simulations [47] and direct measurements [48,49] have revealed the impact of thermal hysteresis and field protocol on the ECE close to phase transitions. Furthermore, field hysteresis and the field direction may strongly influence the ECE in the ferroelectric phase. For instance, based on an analytical model in Ref. [37], it has been found that the overall cooling can be enhanced by field reversal. This concept has been demonstrated by experiments [3,6,37,45,50] and it has been shown that ferroelectric switching and related work losses may result in large modifications of ΔT. However, we are not aware of a study on the impact of the internal bias fields and different field protocols on the ECE.

In the present paper, we combine phenomenological Landau theory [23,51] with *ab-initio*-based molecular dynamics (MD) simulation [52] in order to shed light on the interplay between external and internal field strengths, field protocols, and thermal history in ferroelectrics with internal bias fields. Thereby, we consider reversible and irreversible specific entropy changes. In particular we predict routes to optimize the ECE for a fixed small magnitude of the applied field, which is important for devices where Joule heating and electrical breakdown limit the strength of the external field.

The paper is organized as follows. First, in Sec. II, the model that we use is elaborated. Second, in Sec. III A, the influence of internal bias fields on the ECE is discussed. Hereby, we focus on the impact of different strengths of the internal field, which is antiparallel to the external field. As supplementary information, the impact of the external field strength for a fixed internal field and the trends for parallel external and internal fields are discussed in Appendixes A and B, respectively. In Appendix C, we confirm our predictions for the example of defect dipoles by *ab-initio*-based MD simulations. In Sec. III B, based on the knowledge obtained, we predict how the ECE in the presence of internal bias fields can be optimized by the field protocol. Finally, the conclusions and outlook can be found in Sec. IV.

II. THE ANALYTICAL MODEL

Pirc *et al.* proposed an analytical model to determine the ECE for reversible changes of the polarization based on Landau theory [51]. In Ref. [37], irreversible changes of the polarization in the course of ferroelectric switching have been added to this model. Internal bias fields can be included in the Landau model straightforwardly. For example, fixed defect dipoles induce a polarization P_d parallel to the polarization of their surroundings during equilibration, which couples with the polarization of the free dipoles P and gives rise to the internal electric field E_d. We assume a coupling $E_d = 2JP_d$ with $J = 3.0$. We can define the

mean-field free-energy density F_{dip} as follows:

$$F_{\mathrm{dip}} = F_0 + \frac{1}{2}aP^2 + \frac{1}{4}bP^4 - E_{ex}P - \frac{1}{2}E_dP, \quad (1)$$

where E_{ex} is the external field.

It should be noted that we assume homogeneous internal and external fields. On the one hand, this may be a severe approximation for complex point and line defects. On the other, this model allows us to systematically study the impact of shifted hysteresis on the caloric response and it reproduces the trends for unidirectional local defect dipoles, which are randomly distributed in the sample (cf., Appendix C). According to Kutnjak *et al.*, we use dimensionless quantities ($T_0 = 1$, $b = 1/3$, and $a_0 = \partial a/\partial T = 1$) [10], neglect the temperature dependency of b and E_d, and assume $a = a_0(T - T_0)$, in which T and T_0 are the temperature and the Curie temperature, respectively.

At equilibrium, the free-energy density has a local extremum ($\partial F_{\mathrm{dip}}/\partial P = 0$), resulting in

$$E_{ex} = aP + bP^3 - E_d/2. \quad (2)$$

In the ferroelectric phase ($T < T_0$), the equilibrium $P(E_{ex})$ curve is thus S shaped and between the left and right coercive fields (points E and B in Fig. 1), multiple metastable states exist. In this hysteretic region, changes of the external field induce reversible and irreversible changes of P. As shown experimentally by Bolten *et al.* [53,54], the reversible changes of P are given by a straight line passing through the center of the hysteresis, with a slope of $E(P)$ at the coercive field ($\partial E_{ex}/\partial P\,|_B = a + 3bP_B{}^2$). The reversible polarization P_r and the corresponding field E thus satisfy the relation

$$E_{ex} = aP_r + 3bP_B{}^2P_r - E_d/2. \quad (3)$$

By substituting Eq. (2) into Eq. (3), we obtain the reversible polarization:

$$P_r = \frac{aP + bP^3}{a + 3bP_B{}^2}.$$

If the field is varied between E_{init} and E_{end}, it induces a change in P, which is related to the work density $W_{\mathrm{actual}} = \int_{P_{\mathrm{init}}}^{P_{\mathrm{end}}} E_{ex}dP$, in which P_{init} and P_{end} are the initial and final polarization, respectively. For positive E_{ex}, the work is thus positive if $|P|$ increases, while it is negative if $|P|$ decreases, and vice versa for negative E_{ex}. Outside the hysteretic region (e.g., between A and B or E and G in Fig. 1), the field-induced work is fully reversible. In the hysteretic region (e.g., between B and E in Fig. 1), we can divide the actual work density into the reversible work density done on P_r and the irreversible work-loss density. Without switching of the polarization direction (e.g., between B and D in Fig. 1), the losses are given as follows:

$$\begin{aligned} W_{\mathrm{loss}} &= W_{\mathrm{actual}} - W_r \\ &= \int_{P_B}^{P} E_{ex}dP - \int_{P_{B'}}^{P_r} E_{ex}dP_r \\ &= \frac{1}{2}aP^2 + \frac{1}{4}bP^4 - \left(\frac{1}{2}aP_B{}^2 + \frac{1}{4}bP_B{}^4\right) + \frac{1}{2}aP_{B'}{}^2 \\ &\quad + \frac{3}{2}bP_B{}^2P_{B'}{}^2 - \left(\frac{1}{2}aP_r{}^2 + \frac{3}{2}bP_B{}^2P_r{}^2\right) \\ &\quad - (P - P_B - P_r + P_{B'})E_d/2, \end{aligned} \quad (4)$$

where $P_{B'} = P_r|_{P=P_B} = (aP_B + bP_B^3)/(a + 3bP_B^2)$. In the course of switching (e.g., between D and E in Fig. 1), the losses are furthermore enhanced by $(P - P_D)E_D$. The actual and reversible work densities for a field variation from B to N are illustrated in Fig. 1, in blue and green, respectively. Shifting the green area by $(0,\ P_B - P_{B'})$ allows us to determine the work loss (gray area): compare Figs. 1(a) and 1(b).

As discussed above, the sign of the work depends on the sign of E_{ex} and the change of $|P|$, and thus losses may also be positive or negative. In particular, reducing the external field parallel to P induces negative losses. However, these small losses are negligible without switching of the polarization direction [see Fig. 1(b)]. The losses increase considerably in the course of switching. However, without a bias field, switching is induced by an increasing antiparallel field and thus is commonly related to positive losses. It is a unique feature of systems with internal bias fields that a large loss magnitude (switching) can be combined with a negative sign (reduction of a positive field) if both coercive fields have the same sign [see Fig. 1(c)]. It should be noted that work losses are not reversible and differ between field application and removal. If the field is ramped from G to B, the field increases and is antiparallel to the initial polarization direction [see Fig. 1(d)]. Therefore, the work loss is positive. In comparison to the field change from B to G, the magnitude of the loss increases by the area of the hysteresis (pink). Thus the overall work loss in a full field cycle ($G \rightarrow B \rightarrow G$) is positive and is given by the area of the hysteresis.

Depending on the conditions (isothermal, adiabatic, or mixed), a variation of the external field induces changes of the specific entropy and/or temperature of the system. In order to determine the adiabatic temperature change, it is convenient to separate the specific entropy change into the field-induced reversible (ΔS_{dip}) and irreversible ($\Delta S_{\mathrm{total}} = W_{\mathrm{loss}}/T_{\mathrm{init}}$) changes of the dipolar degrees of freedom, and the remaining vibrational degrees of freedom (S_{vib}), which depend only weakly on the external field [10,37,51]:

$$\Delta S_{\mathrm{vib}} = \Delta S_{\mathrm{total}} - \Delta S_{\mathrm{dip}}. \quad (5)$$

$S_{\rm dip}$ is given as follows:

$$\begin{aligned}\Delta S_{\rm dip} &= S_{\rm dip}(P) - S_{\rm dip}(P_{\rm init}) \\ &= -\frac{1}{2}a_0(P^2 - {P_{\rm init}}^2),\end{aligned} \tag{6}$$

where $S_{\rm dip} = -\partial F_{\rm dip}/\partial T = -\frac{1}{2}a_0P^2$.

Neglecting the weak temperature dependency of the specific heat capacity of the nonpolar degrees of freedom [55], $c_{\rm ph}$ is taken as 15 in the reduced units according to Ref. [51]. The change of the specific vibrational entropy is given, by the initial $T_{\rm init}$ and final temperature $T_{\rm end}$, as

$$\Delta S_{\rm vib} = \int_{T_{\rm init}}^{T_{\rm end}} \frac{c_{\rm ph}}{T} dT \cong c_{\rm ph} \ln(T_{\rm end}/T_{\rm init}), \tag{7}$$

and the adiabatic temperature change can be determined by

$$\Delta T = T_{\rm init} \exp[(W_{\rm loss}/T_{\rm init} - \Delta S_{\rm dip})/c_{\rm ph}] - T_{\rm init}. \tag{8}$$

For a discussion of the temperature dependency of the ECE, it is convenient to define two characteristic temperatures for each combination of external and internal fields. At low temperatures, the field hysteresis is broad and thus $E_c^{\rm left}$ is negative and $E_c^{\rm right}$ is large, and potentially exceeds the applied field E_{ex}. With increasing temperature, the hysteresis is systematically reduced, i.e., $E_c^{\rm left}$ and $E_c^{\rm right}$ increase and decrease, respectively. At T', the left coercive field changes sign, and at T'' the external field exceeds $E_c^{\rm right}$ (see Fig. 2). The polarization at the coercive fields is given as $P_{D,F} = \pm\sqrt{-a/3b}$. According to Eq. (2), the left and right coercive fields are thus given as

$$\begin{aligned}E_c^{\rm left} &= \frac{2}{3}a\sqrt{-\frac{a}{3b}} - E_d/2, \\ E_c^{\rm right} &= -\frac{2}{3}a\sqrt{-\frac{a}{3b}} - E_d/2,\end{aligned} \tag{9}$$

resulting in characteristic temperatures of

$$\begin{aligned}T' &= T_0 - (-E_d/2)^{2/3}(27b/4)^{1/3}/a_0, \\ T'' &= T_0 - (E_{\rm init} + E_d/2)^{2/3}(27b/4)^{1/3}/a_0.\end{aligned} \tag{10}$$

III. RESULTS AND DISCUSSION

In the following, we discuss systematically how antiparallel internal fields modify the ECE. Hereby, we show that the ECE depends on the relative strength of the external and internal fields. In Sec. III A, we realize different ratios of both fields by a variation of the bias field (E_d) for the removal of an external field with fixed magnitude ($E_{\rm init} = 0.2$ and $E_{\rm end} = 0$). As supplementary information, the variation of the external field for a fixed induced bias field ($E_d = -0.6$) is discussed in Appendix A.

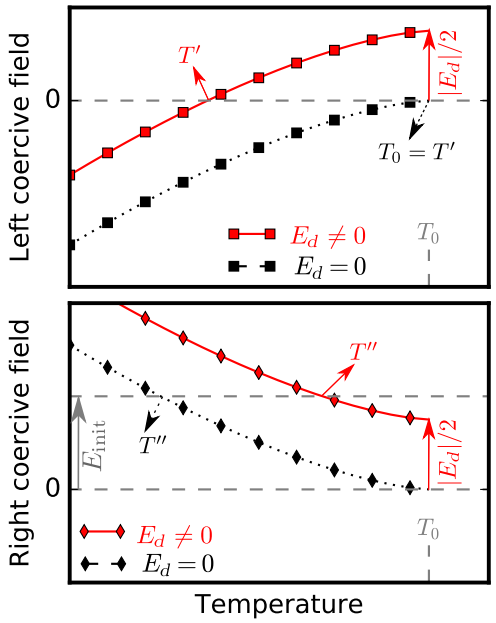

FIG. 2. Characteristic temperatures T' and T'', determined by the external fields $E_{\rm init}$ and the variation of the left and right coercive fields ($E_c^{\rm left}$, $E_c^{\rm right}$) with temperature (see Fig. 1). T' indicates the temperature at which $E_c^{\rm left} = 0$, without bias fields (dashed lines with black squares) and for an induced bias field E_d (solid lines with red squares). T'' indicates the temperature at which $E_c^{\rm right} = E_{\rm init}$, without bias fields (dashed lines with black diamonds) and for an induced bias field E_d (solid lines with red diamonds).

A. The influence of internal bias fields

It is convenient to discuss the systematic trends for five representative strengths of the internal field: (i) no internal bias field ($E_d = 0$) as shown in Fig. 3, (ii) a weak internal field $|E_d| < E_{\rm init}$ as shown in Fig. 4, (iii) equal magnitudes of the fields $|E_d| = E_{\rm init}$ as shown in Fig. 5, (iv) a stronger internal field $|E_d| > E_{\rm init}$ as shown in Fig. 6, and (v) a very strong internal field $|E_d| = 2E_{\rm init}$ as shown in Fig. 7. Furthermore, the systematic reduction of the field hysteresis with temperature results in three different temperature ranges: low temperatures (no switching of the polarization direction), intermediate temperatures (switching of the polarization direction), and high temperatures (paraelectric phase without field hysteresis).

1. Low temperatures: all cases

The general trends for positively poled samples and $T < T'$ can be summarized as follows. The polarization is on the upper branch of the field hysteresis with and without the positive field. Therefore, losses are negligible during field ramping [cf., green triangles in Figs. 3–7(b)], and the ECE is dominated by the reversible change of the specific dipolar entropy. For field removal, $P_{\rm end} < P_{\rm init}$, i.e., the specific dipolar entropy increases (cf., Eq. (6)) and the

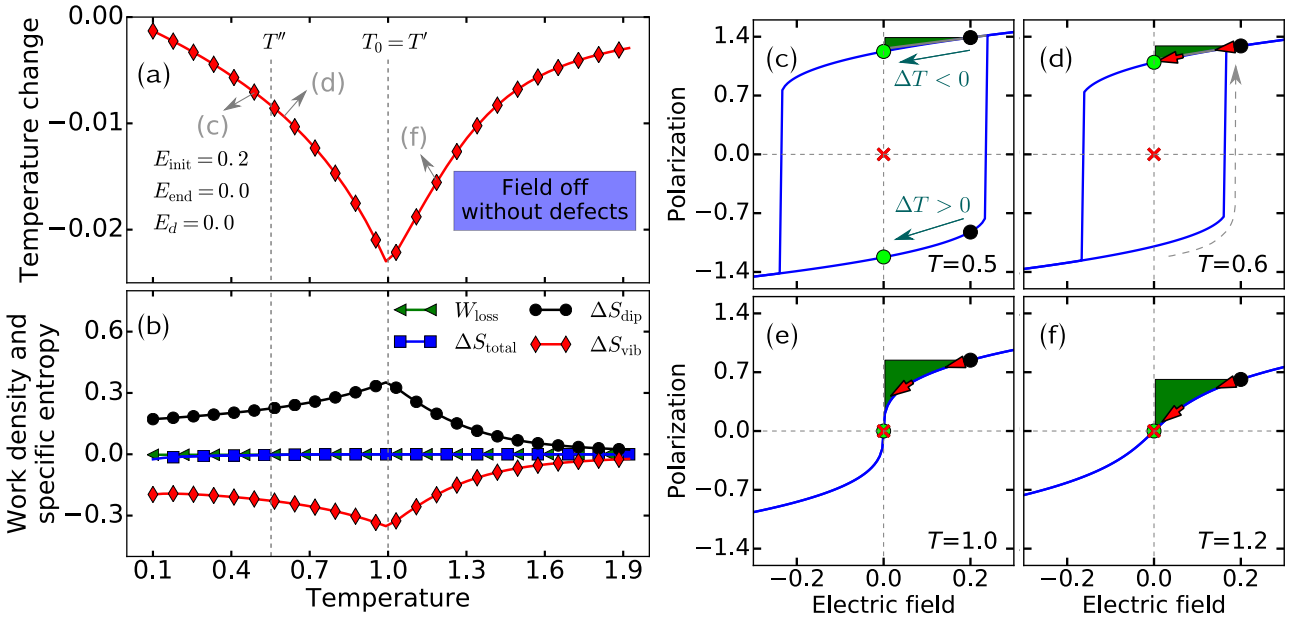

FIG. 3. Case (i)—the electrocaloric effect without an internal bias field in the sample with positively poled initial states: (a) the temperature change ΔT; (b) the corresponding work-loss density and specific entropy changes; (c)–(f) representative hysteresis loops. In (c)–(f), the dots, crosses, and arrows illustrate the initial and final states, the center of the hysteresis, and the direction of the field change. Ramping off the field, (c) demonstrates the conventional ECE on the upper branch, and the inverse ECE on the lower branch.

system cools down under adiabatic conditions. Analogous field application reduces the specific dipolar entropy, and the system heats up, i.e., a reversible conventional ECE is observed.

For negatively poled samples, the trends for $T < T''$ in Figs. 3–7 are analogous. In all cases, the polarization is on the lower branch of the field hysteresis with and without the positive field, losses are negligible, and the

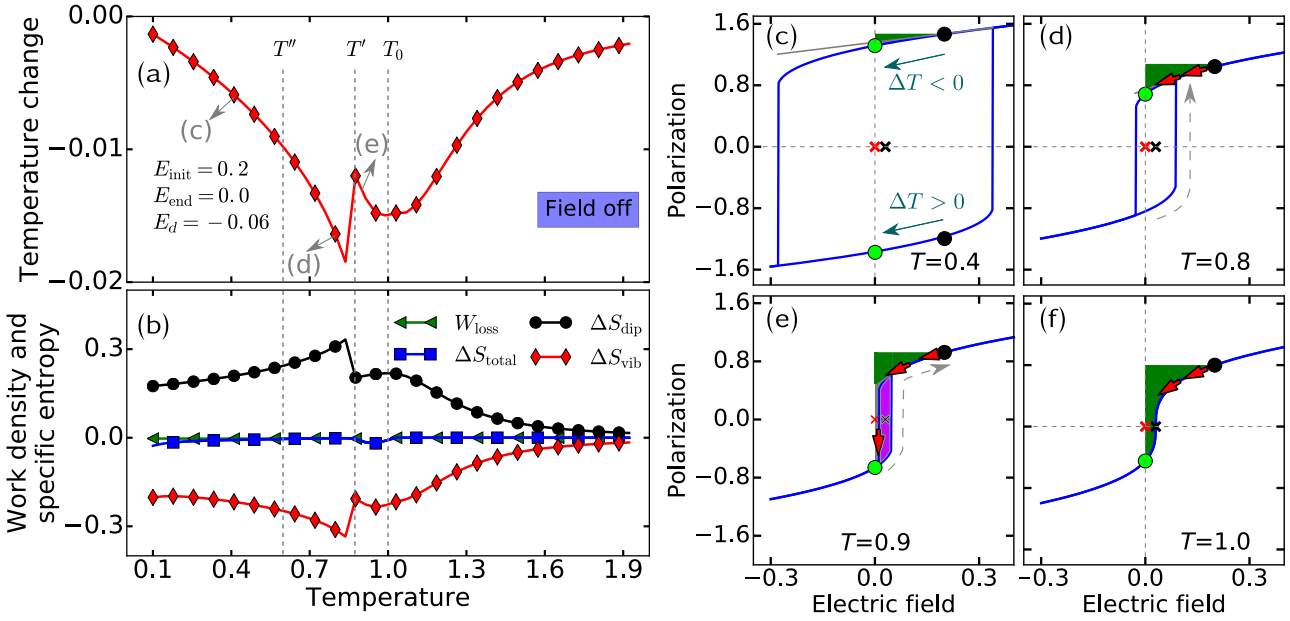

FIG. 4. Case (ii)—the electrocaloric effect for weak internal bias fields $0.06 = |E_d| < E_{\rm init} = 0.2$ in the sample with positively poled initial states: (a) the temperature change ΔT; (b) the corresponding work-loss density and specific entropy changes; (c)–(f) representative hysteresis loops. In (c)–(f), the dots, crosses, and arrows illustrate the initial and final states, the center of the hysteresis, and the direction of the field change. Ramping off the field, (c) demonstrates the conventional ECE on the upper branch, and the inverse ECE on the lower branch.

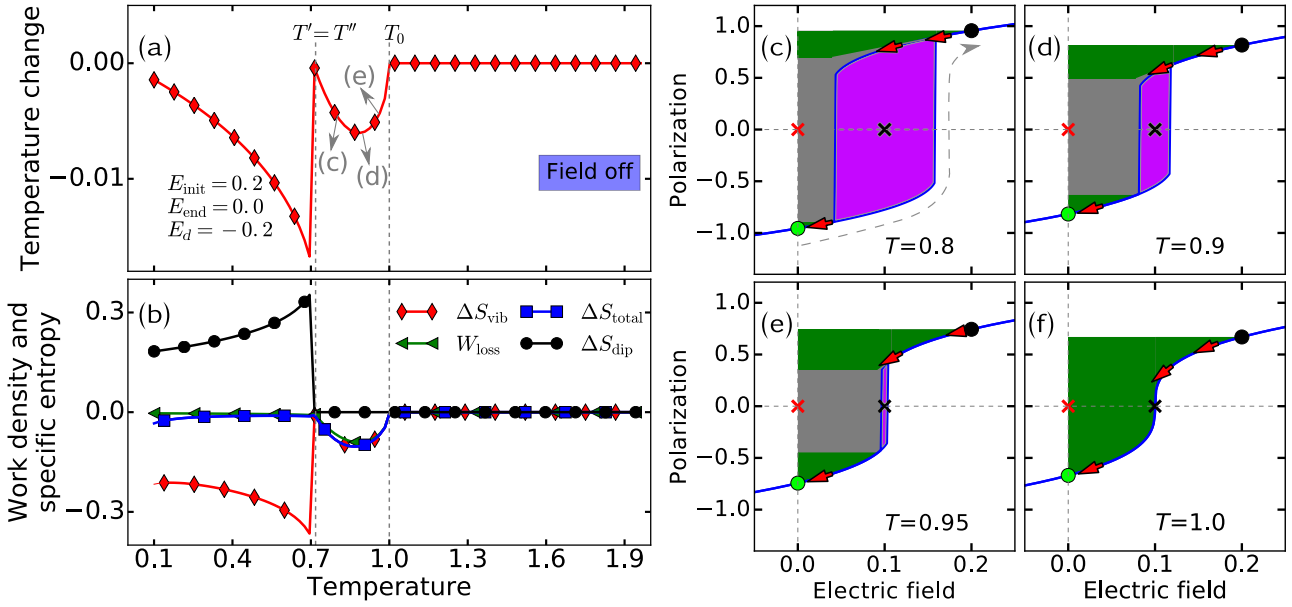

FIG. 5. Case (iii)—the electrocaloric effect for equal internal and external field strengths ($|E_d| = E_{\rm init} = 0.2$) in the sample with positively poled initial states: (a) the temperature change ΔT; (b) the corresponding work-loss density and specific entropy changes; (c)–(f) representative hysteresis loops. In (c)–(f), the dots, crosses, and arrows illustrate the initial and final states, the center of the hysteresis, and the direction of the field change.

ECE is dominated by the reversible change of the specific dipolar entropy. As $|P_{\rm end}| > |P_{\rm init}|$ for field removal, the system heats up, and vice versa for field application, i.e., a almost reversible inverse ECE occurs. For field removal, Figs. 3(c) and 4(c) demonstrate the exemplary cases, with the conventional ECE on the upper branch and the inverse ECE on the lower branch.

With increasing strength of the internal field, T' decreases from 1.0 to 0.873, 0.718, 0.630, and 0.552 for cases (i), (ii), (iii), (iv), and (v), respectively (cf., Eq. (10)).

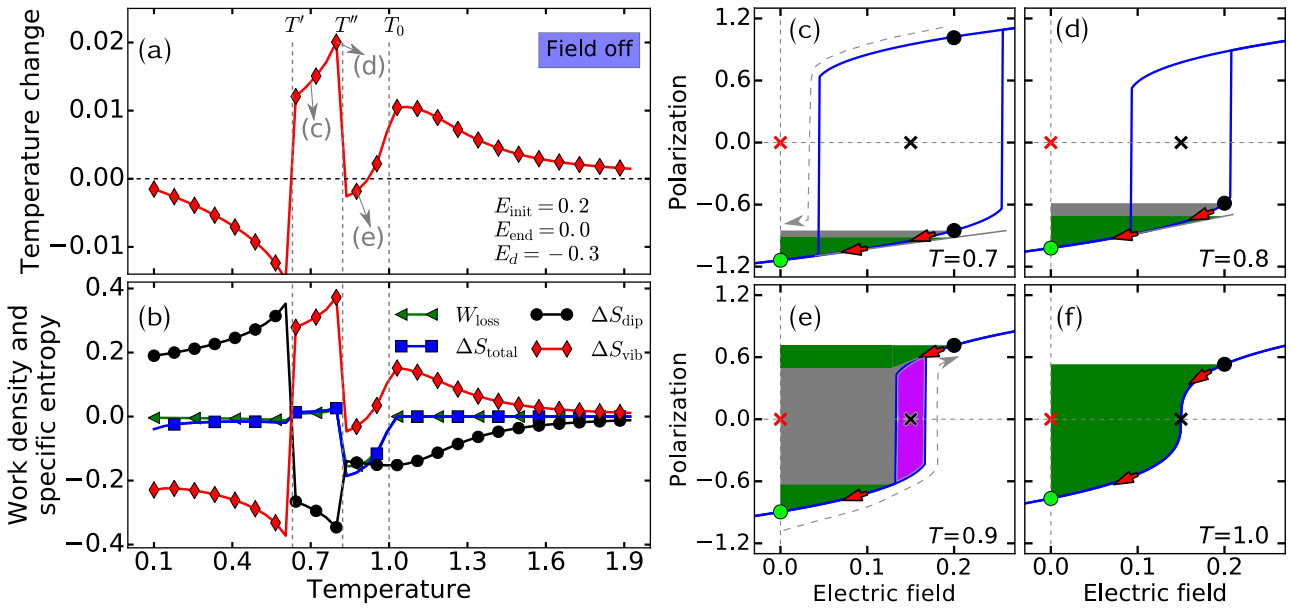

FIG. 6. Case (iv)—the electrocaloric effect for stronger internal bias fields ($0.3 = |E_d| > E_{\rm init} = 0.2$) in the sample with negatively initial poled states for $T' < T < T''$, and positively initial poled states for all other values of T: (a) the temperature change ΔT; (b) the corresponding work-loss density and specific entropy changes; (c)–(f) representative hysteresis loops. In (c)–(f), the dots, crosses, and arrows illustrate the initial and final states, the center of the hysteresis, and the direction of the field change.

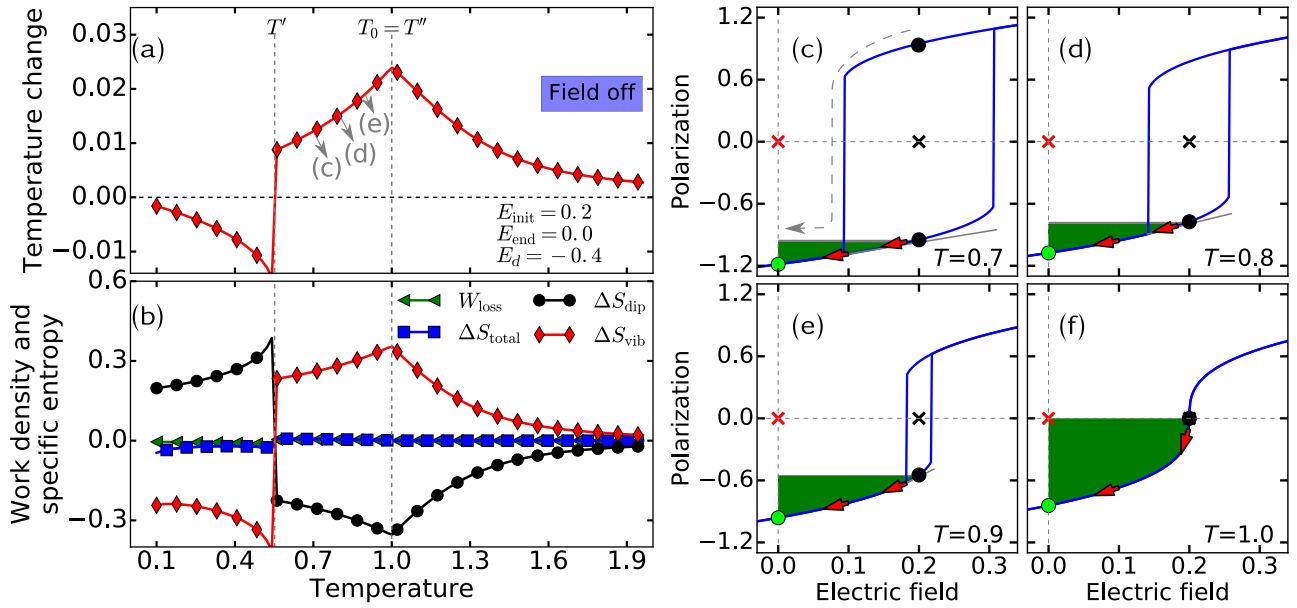

FIG. 7. Case (v)—the electrocaloric effect for strong internal bias fields ($|E_d| = 2E_{\rm init} = 0.4$) in the sample with positively initial poled states for $T < T'$ and negatively initial poled state for $T > T'$: (a) the temperature change ΔT; (b) the corresponding work-loss density and specific entropy changes; (c)–(f) representative hysteresis loops. In (c)–(f), the dots, crosses, and arrows illustrate the initial and final states, the center of the hysteresis, and the direction of the field change.

At the same time, T'' increases with the ratio of the internal to the external field; i.e., for a field strength of $E_{\rm init} = 0.2$, we find $T'' = 0.552$, 0.598, 0.718, 0.822, and 1 in cases (i), (ii), (iii), (iv), and (v), respectively.

Thus, with an increasing strength of the bias field, the temperature ranges with a reversible conventional ECE decease, while the ranges with an inverse ECE increase.

Well below the Curie temperature, the external field can only sample small changes of P [cf., Fig. 4(c)]. In turn, the ECE is small [56]. With increasing T, the hysteresis narrows and the field samples larger changes of P. Therefore, both the conventional ECE for positively poled samples at $T < T'$ and the inverse ECE for negatively poled samples at $T < T''$ increase with temperature (cf., Figs. 3–7).

2. High temperatures: all cases

For $T > T_0$, the system is in the paraelectric phase, and thus neither work losses nor the previous poling have an impact on the ECE. We note that our simple Landau model does not account for the shift of the ECE peak to higher temperatures with increasing field strength, as commonly observed in experiments and MD simulations.

Field application and removal always result in fully reversible changes of P and a reversible ECE. In agreement with the predictions in Ref. [10], ΔP decreases systematically with increasing temperature and the ECE is maximal at $T = T_0$ [see Fig. 3(a)].

The largest conventional ECE is observed for the ideal material ($P_{\rm init} > 0$, $P_{\rm end} = 0$). An increasing internal field induces an increasing negative polarization ($P_{\rm end} < 0$) and thus systematically lowers the conventional ECE (cf., Figs. 3 and 4). For $|E_d| = E_{\rm init}$, both the positive polarization along the external field and the negative polarization parallel to the internal field have the same magnitude ($P_{\rm init} = -P_{\rm end}$): thus the ECE vanishes (see Fig. 5). For a further increase of $|E_d|$, the negative polarization without any field and thus the inverse ECE increase systematically (cf., Figs. 5–7).

Thus, for both low and high temperatures, the relative strengths of both fields determine the magnitude and the sign of the reversible ECE. Antiparallel internal fields systematically reduce the conventional ECE, whereas the opposite holds for the inverse ECE.

3. Intermediate temperatures

For intermediate temperatures, already unipolar field cycling induces the switching of the polarization direction from the upper to the lower branch ($T' < T < T_0$), and from the lower to the upper branch ($T'' < T < T_0$), giving rise to a complex dependency of the ECE on the relative field strengths and previous poling.

Case (i): $|E_d| = 0$.—Without internal bias fields and for the chosen strength of the external field, the characteristic temperatures order as $T'' < T' = T_0$ (cf., Eq. (10)). Ramping on a positive field on a negatively poled sample in the temperature range $T'' < T < T'$ induces the switching of the polarization direction [cf., the gray dashed arrow in Fig. 3(d)]. This switching reduces $\Delta|P|$ and in turn $\Delta S_{\rm dip}$.

Furthermore, positive work losses are induced. However, this response is not accessible in a cycling field, as the system would stay in the positively poled state after the first field pulse. Hence, this response is not useful in a cooling device.

Case (ii): $|E_d| < E_{\text{init}}$.—Already weak bias fields (e.g., $|E_d| = 0.06$) modify the characteristic temperatures ($T'' < T' < T_0$), and impose strong modifications of the ECE (see Fig. 4).

For $T' < T < T_0$, the cycling of the unipolar field results in a repeatable switching between the positive and negative polarization directions. As the switching reduces $\Delta|P|$ and in turn ΔS_{dip}, ΔT is abruptly reduced at T', compared to the response at lower T.

As the left coercive field is small for weak bias fields, W_{loss} and ΔS_{total} are negligible, particularly for field removal. Although the positive work-loss density increases by the area of the field hysteresis for field application (see Sec. II), this area is small, as $T' \lesssim T_0$ [see Fig. 4(e)]. Thus no large differences in $|\Delta T|$ are to be expected between cooling and heating in a cycling field.

Analogous tendencies of specific dipolar entropy change and work-loss density occur for field application in a negatively poled sample with $T'' < T < T'$ [not shown in Fig. 4(a)]. Here, an increasing work-loss density is to be expected with decreasing T, due to the increasing width of the thermal hysteresis. As discussed in case (i), the corresponding ECE is, however, only relevant for the first field pulse and would irreversibly heat up the material [cf., the gray dashed arrow in Fig. 4(d)].

With increasing strength of the internal bias field, the specific dipolar entropy change for $T > T'$ is systematically reduced. The losses and their difference for field application and removal increase systematically.

Case (iii): $|E_d| = E_{\text{init}}$.—When the internal bias field reaches the external field strength, $\Delta|P|$ for the field-induced switching of the polarization direction is zero and $T'' = T'$. Hence, ΔS_{dip} is zero in the intermediate-temperature regime and there is no difference between previous positive or negative poling. Nevertheless, the work losses induce a finite cooling of the material under field removal (conventional ECE). As discussed in Sec. II, this counterintuitive trend is related to the positive left coercive field and the resulting negative work loss. The temperature dependency of the losses for field removal is illustrated by the gray areas in Figs. 5(c)–5(e). With increasing T, due to the reduction of thermal hysteresis and irreversible polarization changes, the width of the gray area increases, while the height decreases. This results in a local maximum of the losses and the corresponding ECE between T' and T_0 [see Figs. 5(a)].

It should be noted that $|W_{\text{loss}}|$ is further increased for field application due to the finite width of the field hysteresis [cf., the gray dashed arrows in Fig. 5(c)]. Therefore, the heating found for field application exceeds the cooling for field removal due to the extra work losses [cf., the pink areas in Figs. 5(c)–5(e)]. Due to the reduction of thermal hysteresis with T, this difference gradually vanishes.

Case (iv): $|E_d| > E_{\text{init}}$.—As soon as the internal field exceeds the external field, T'' is larger than T' (cf., Eq. (10)). For $T'' < T < T_0$, the polarization direction switches for application and removal of the positive field, and the previous poling of the sample has no impact on the ECE. As $|E_d| > E_{\text{init}}$, the negative polarization without an external field exceeds the positive polarization induced by the external field [see Fig. 6(e)]. Thus ΔS_{dip} is negative (inverse ECE) and has a local extremum at T_0. At the same time, a conventional ECE is induced by the losses. As $|W_{\text{loss}}|$ is maximal at T'' and gradually decreases to zero at T_0, the net temperature change under field removal varies from a small negative value (conventional ECE) around T'' to a large positive value (inverse ECE) at T_0.

As discussed above, field application induces larger losses [cf., the gray dashed arrow and the pink area in Fig. 6(e)] and, in particular, close to T'', an enhanced net conventional ECE would occur, heating up the sample. With increasing T, the thermal hysteresis vanishes and thus the difference between field application and removal also becomes negligible.

We note that the same trends (switching of the polarization direction and superimposed inverse and conventional ECE) also occur for the removal of the field from a positively poled sample for $T' < T < T''$ [cf., the gray dashed arrow in Fig. 6(c)]. However, in this temperature range further cycling of the field cannot induce the back switching of the polarization. Hence, the reversible inverse ECE discussed for negatively poled samples occurs in successive field cycles (cf., the red arrows).

Case (v): $|E_d| = 2E_{\text{init}}$.—With an increasing ratio of the internal to the external field strength, T'' increases systematically and, finally, for $|E_d| = 2E$, $T'' = T_0$. In this case, a reversible inverse ECE related to S_{dip} is possible for $T' < T < T_0$ in the negatively poled sample.

As discussed for weaker bias fields, a conventional ECE with large contributions of work losses is also possible for field removal from a positively poled sample for $T > T'$, which is, however, only accessible in the first field cycle, as $E < E_c^{\text{right}}$, referring to the gray dashed arrow in Fig. 7(c).

In summary, both conventional and inverse ECE can be found in all ferroelectric materials for $T < T_0$ and positively and negatively poled initial states, respectively.

In the presence of bias fields, the ECE depends crucially on the relative strength of the external and the bias field and on temperature. First, for positively poled initial states, the bias fields reduce the temperature range and the magnitude of the reversible conventional ECE ($|E_{\text{init}}| > |E_d|$). Second, for negatively poled initial states, the bias fields increase the temperature range related to a reversible inverse ECE ($|E_{\text{init}}| < |E_d|$). Furthermore, ΔT of

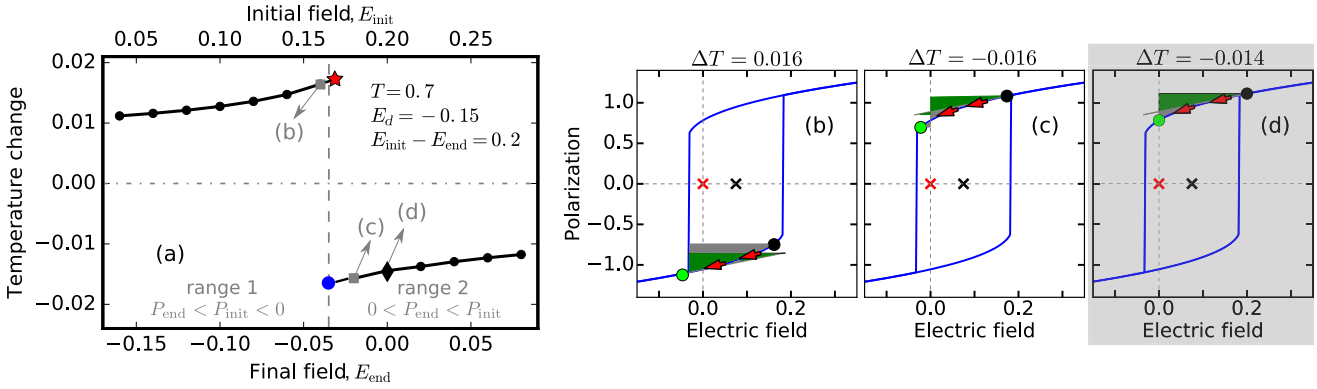

FIG. 8. The impact of the field protocols on the temperature change for $T < T'$ and $E_{\rm init} > E_{\rm end}$ for case (ii)—weak internal bias fields ($T = 0.7$, $E_d = -0.15$): (a) the temperature change for different field ranges; (b)–(d) representative hysteresis for the data points marked in gray [the highlighted data points are used for Fig. 11(a)]. The red star and blue dot represent ΔT, using design options 1 and 2, respectively.

the inverse ECE increases with an increase of the internal bias field.

For intermediate temperatures, the polarization direction switches, which reduces the dipolar entropy change and induces large losses. Notably, negative losses, i.e., the cooling of the material, occur for field removal and positive left coercive fields. However, the losses depend crucially on the direction of the field change. As the positive loss for field application exceeds the negative loss for field removal, in the absence of proper heat ejection to the surroundings, a cycling field would induce an irreversible heating of the sample. The same trends are found if we change $E_{\rm init}$ for fixed E_d (see Appendix A).

We note that the observed temperature- and field-dependent transition between a conventional and an inverse ECE is in agreement with the trends which have been observed in Monte Carlo and MD simulations [22,23]. In particular, considering the different magnitudes of the corresponding losses, i.e., the total entropy change, the results allow us to interpret the larger conventional ECE found for field application than for removal.

B. The impact of the field protocol

In the following section, we use the knowledge gained to tailor the ECE according to the field protocol, i.e., the initial and final field strengths for a fixed field interval of $E_{\rm init} - E_{\rm end} = 0.2$. We focus on initial field strengths and polarization directions, which are accessible by a cycling electrical field of the chosen magnitude. With $E_{\rm init} > E_{\rm end}$, for case (ii), weak internal bias fields $|E_d| < |\Delta E_{ex}|$, and case (iv), strong internal bias fields $|E_d| > |\Delta E_{ex}|$, the results are summarized in Figs. 8–10. Note that we have chosen slightly different values of the internal bias fields compared to the previous section in order to underline the general validity of our discussion.

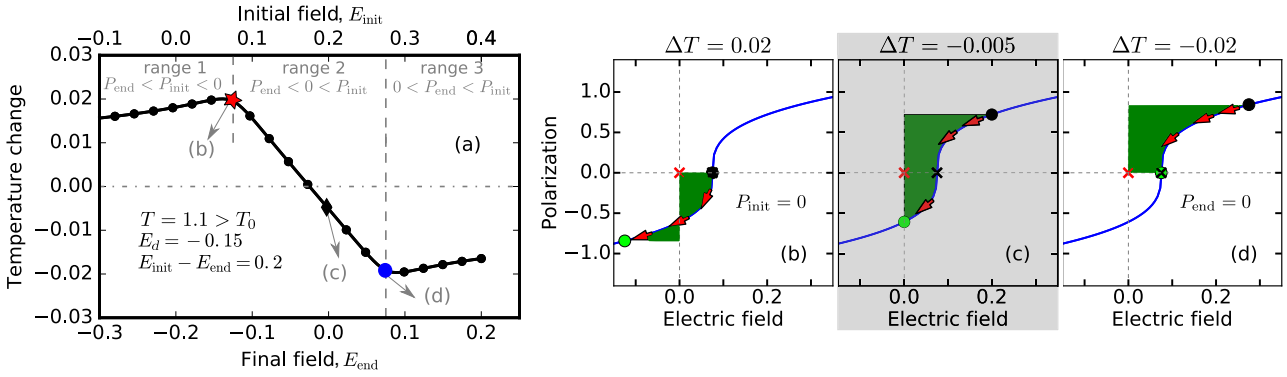

FIG. 9. The impact of the field protocols on the temperature change for $T > T_0$ and $E_{\rm init} > E_{\rm end}$ for case (ii)—weak internal bias fields ($T = 1.1$, $E_d = -0.15$): (a) the temperature change for different field ranges; (b)–(d) representative hysteresis for the data points marked in gray [the highlighted data points are used for Fig. 11(a)]. The red star and blue dot represent ΔT, using design options 3 and 4, respectively.

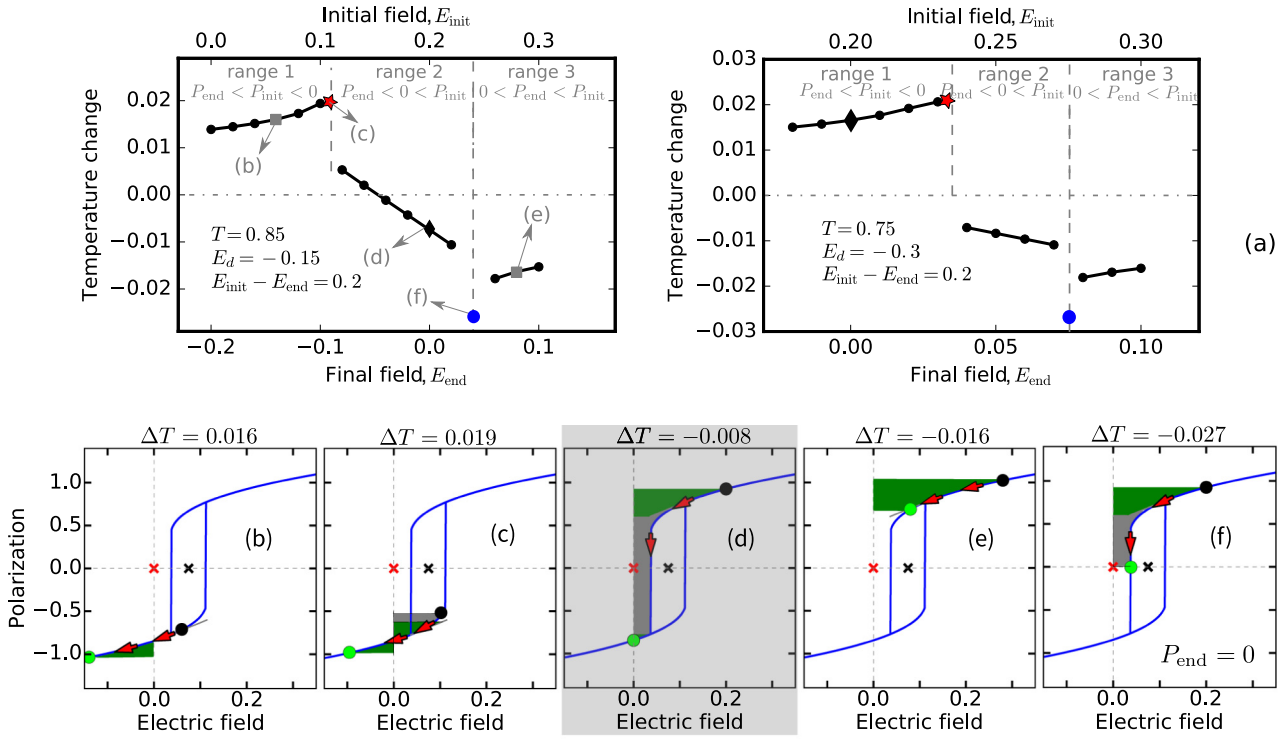

FIG. 10. The impact of the field protocols on the temperature change for $T' < T < T_0$ and $E_{init} > E_{end}$. (a) The temperature change for different field ranges. Left, case (ii)—weak internal bias fields ($T = 0.85$, $E_d = -0.15$); right, case (iv)—strong internal bias fields ($T = 0.75$, $E_d = -0.3$). (b)–(f) Representative hysteresis for the data points marked in gray for case (ii) [the highlighted data points are used for Fig. 11(a)]. The red star and blue dot represent ΔT, using design options 1 and 5, respectively.

1. Low temperatures ($T < T'$)

At low temperatures, we can depict two field intervals giving rise to repeatable and reversible responses in a cycling field. For $E_{ex} < E_c^{right}$, the system is on the lower branch of the hysteresis: reversible heating is found for $E_{init} > E_{end}$ and cooling for $E_{init} < E_{end}$. By contrast, for $E_{ex} > E_c^{left}$, the system is on the upper branch: reversible heating is found for $E_{init} < E_{end}$ and cooling for $E_{init} > E_{end}$.

Both responses can be systematically enhanced if the field samples the parts of the hysteresis with a larger slope, i.e., if the field interval is shifted to the right for negatively poled samples, or if the field interval is shifted to the left for positively poled samples, as illustrated in Fig. 8(c). Although ramping the field to the coercive fields ($P_{end} = 0$) optimizes the dipolar entropy change for both polarization directions, at the same time positive work losses are induced, and thus an irreversible heating of the sample occurs. These findings are in agreement with the enhancement of the ECE by reversed fields and its reduction by losses in the course of switching found for materials without bias fields [37,45], and are also verified by MD simulations (cf., Appendix C).

In summary, for low temperatures ($T < T'$) and $E_{init} > E_{end}$, the maximal caloric heating for positively poled initial states is found for ramping from the shoulder of the hysteresis (design option 1) [cf., the red star in Fig. 8(a)], while the maximal caloric cooling for negatively poled initial states is found for ramping to the shoulder of the hysteresis (design option 2) [cf., the blue dot in Fig. 8(a)].

2. High temperatures ($T \geq T_0$)

In the paraelectric phase, the response is fully reversible and three field ranges can be depicted (see Fig. 9).

In field range 1, for $E_{ex} < |E_d|/2$ the system is poled along the negative direction. Thus, the system heats up for $E_{init} > E_{end}$ and cools down for $E_{init} < E_{end}$. In field range 3, for $E_{ex} > |E_d|/2$ the system is poled along the positive direction. Thus, the system cools down for $E_{init} > E_{end}$ or heats up for $E_{init} < E_{end}$. For intermediate field strengths, the polarization direction switches for both directions of the field change.

The ECE can be maximized if the field samples the interval with the largest slope of the polarization. Thus, the caloric heating for negative polarization can be systematically enhanced if the field interval is shifted to the right and is maximal if it approaches $|E_d|/2$ (design option 3) [cf., the red cross in Fig. 9(a)]. Analogously, the caloric cooling for positive polarization can be systematically enhanced if the field interval is shifted to the left and is maximal if it

approaches $|E_d|/2$ (design option 4) [cf., the blue dot in Fig. 9(a)].

However, in both cases, if the field interval exceeds the switching field, $\Delta|P|$ and the ECE are systematically reduced. If the field interval is symmetric with respect to $|E_d|/2$, i.e., for $E_{\text{init}} + E_{\text{final}} = |E_d|$, the polarization switches with $\Delta|P| = 0$ and there is no ECE. Thus, the external field interval has to be chosen carefully in order to obtain maximal cooling or heating.

3. Intermediate temperatures ($T' < T < T_0$)

The results for the ferroelectric phase and intermediate temperatures are summarized in Fig. 10. Analogous to the low-temperature range $T < T'$, the maximal reversible heating responses for the negatively poled sample can be found if the field interval is shifted to the shoulder point of the hysteresis and $E_{ex} < E_c^{\text{right}}$ (design option 1) [cf., the red star in field range 1 of Fig. 10(a)]. Analogously, the maximal cooling response for the positively poled material can be optimized if the field interval is shifted to the shoulder of the hysteresis and $E_{ex} > E_c^{\text{left}}$ (design option 2) in field range 3 of Fig. 10(a). For both cases, reversing the direction of the field change reverses the sign of the response. With an increasing initial temperature, field ranges 1 and 3 shift to the left and right, respectively. Meanwhile, an intermediate field range 2 appears.

In this field range 2, the polarization direction switches with $P_{\text{end}} < 0 < P_{\text{init}}$ for $E_{\text{end}} < E_{\text{init}}$. Different from the sole systematic change of the dipolar entropy with the field interval discussed for the paraelectric phase, the switching of the polarization direction induces large work losses. Due to the large change of P in the course of switching, the losses are governed by the small field interval close to E_c. For $T > T'$, the left coercive field is positive and thus losses further cool the material for $E_{\text{end}} < E_{\text{init}}$.

This opens up the possibility of combining work-loss and optimal-dipolar-entropy change in order to obtain a maximal overall cooling (design option 5) [cf., the blue dots in Figs. 10(a) and 10(f)]. First, the dipolar-entropy change is maximal for $P_{\text{end}} = 0$, i.e., for $E_{\text{end}} = E_c^{\text{left}}$. Second, the field-induced change of P is related to an enhanced negative work loss. If P_{end} were to be switched to the negative direction, the negative losses would be further enhanced, contributing more to the overall cooling. However, at the same time the dipolar entropy change would be reduced. Therefore, the point of maximal cooling might appear beyond E_c^{left}, and depends crucially on the material systems, field strengths, and temperatures. For simplicity, this is not discussed in the current paper.

Design option 5 is a unique feature of systems with internal bias fields antiparallel to the initial poling. In contrast, the work loss is positive without bias fields, as discussed in Sec. II and thus induces irreversible heating. In addition, the inverse ECE found on the lower branch of the field hysteresis also cannot be optimized by design option 5. In this case, the cooling found for the opposite direction of the field change would be reduced by the positive work loss. We note that design option 5 can always enhance the cooling response for a positively poled initial state and $0 < E_{\text{end}} < E_c^{\text{left}}$. For $E_{\text{init}} < E_c^{\text{right}}$, the response is, however, not repeatable for a cycling field of the chosen interval. A similar irreversible response may be found at first-order phase transitions (thermal hysteresis) [47]. Furthermore, as discussed in the previous section, the work loss for the reversed field direction imposes an even larger heating of the sample. Regarding this apparent difference of heating and cooling, considerable attention should be paid to the thermodynamic design of devices, which is beyond the scope of this paper.

The same trends can be found for weak and strong bias fields [cf., the left and right parts of Fig. 10(a)]. Thus, in both cases, all three field ranges and comparable maximal cooling and heating occur. However, the different magnitudes of the internal field strengths induce a shift of the field intervals to positive fields.

In summary, the reversible ECE can be found for ramping from or to zero polarization ($T > T_0$), or for ramping

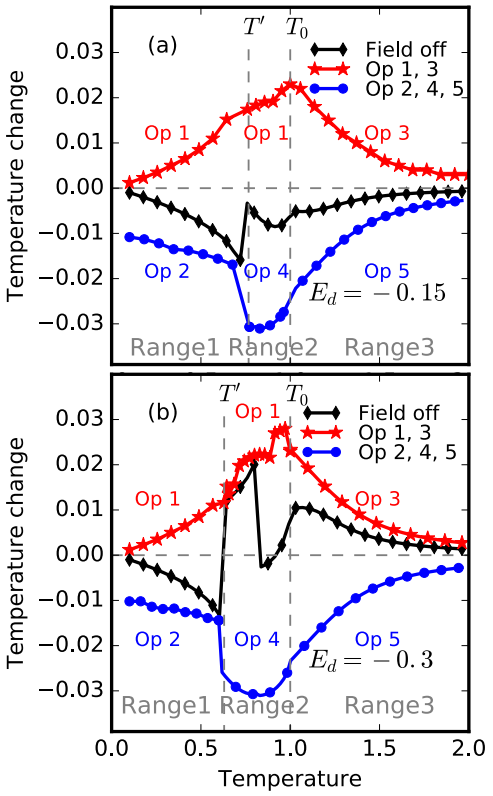

FIG. 11. ECE with $E_{\text{init}} - E_{\text{end}} = 0.2$ for internal bias fields (a) $E_d = -0.15$ and (b) $E_d = -0.3$. Black, $E_{\text{end}} = 0$, for the initial poling direction discussed in Sec. III A. Red, design options 1 and 3 with an optimized heating response. Blue, design options 2, 4, and 5 with an optimized cooling response.

from or to the shoulder of the hysteresis ($T < T_0$). Furthermore, the cooling can be enhanced by the irreversible work loss for $T' < T < T_0$, i.e., positive left coercive fields. The optimized ECE for $E_{\text{init}} > E_{\text{final}}$ is compared to the response found for simple field removal in Fig. 11. For simplicity, only those responses which give rise to a repeatable cooling in a cycling field of the given field strength are included.

Obviously, the proposed design strategies allow us to considerably modify the ECE. First, the reduction of the ECE by internal bias field found for simple field removal can be avoided, comparing black with red and blue lines. Second, for small field strengths, the optimized cooling in the ferroelectric phase ($T < T_0$), i.e., in an attractive temperature range for most applications, can compete with the ECE for $T > T_0$. In particular, the combination of reversible and irreversible contributions (design option 5) allows for a large cooling over a broad temperature range, which broadens further with increasing internal fields. Third, even the sign of the response can be reversed by choosing proper field intervals.

As discussed in Refs. [23,41], we can enhance the ECE by using a combination of inverse and conventional ECE. Based on the results discussed above, according to design options 1 and 3, the optimal cooling can be obtained for $E_{\text{init}} < E_{\text{final}}$, and can be combined with the optimal cooling though design options 2, 4, and 5 for $E_{\text{init}} > E_{\text{final}}$. Additionally, we can broaden the overall temperature span with large ECE by introducing internal bias fields.

IV. CONCLUSION

We study the ECE in the presence of internal bias fields and reveal the complex dependency of the response on temperature, relative field strengths, and the field protocol. In the paraelectric phase, or if the system is on one branch of the ferroelectric hysteresis without switching of the polarization direction, the ECE is dominated by the reversible change of the dipolar entropy. In the case of antiparallel internal bias fields and external fields, the relative strength of both fields determines the magnitude and the sign of the ECE. On the one hand, this allows us to sample the field interval with the largest slope of $P(E_{ex})$ with unipolar fields. This is beneficial as we can enhance the ECE without an increase of E_{ex}, and thus we can avoid ferroelectric breakdown and reduce Joule heating. On the other hand, already weak internal bias fields may considerably reduce the conventional ECE if the field interval is not optimized carefully. If the internal field exceeds the external field strength, a large inverse ECE can be induced. In case of parallel internal fields, the conventional ECE is most relevant (see Appendix B). Thus, the combination of conventional and inverse ECE allows us to enhance the overall ECE by field reversal.

In the case of ferroelectric switching, the work loss is commonly positive and induces irreversible heating of the material. Notably, internal bias fields allow for switching of the polarization direction without field reversal and thus for large negative losses. These losses induce a cooling of the material which is repeatable in a cycling field. Although this additional cooling is irreversible by definition, and even greater heating is found for back switching under field application, it may have the potential to enhance the overall cooling in a optimized thermodynamic cycle as long as the additionally generated heat can be ejected properly.

As summarized in Table I, we propose various strategies to enhance the overall responses for different temperatures by means of the field protocol. First, we can switch between conventional and inverse ECE by a shift of the field interval. Furthermore, we can enhance the overall reversible responses if the field interval is adjusted to the part of the hysteresis showing the largest slope. It is important to realize that the temperature dependency of the thermal hysteresis results in a large temperature dependency of the optimal field intervals, and simple unipolar field cycling may result in unindented switching of the polarization direction, degeneration of the ECE, or even the reversal of the induced temperature change.

We note that our analytical model does not depend on the specific origins of the internal bias fields and is thus probably applicable to a broad class of systems such as ferroelectrics with unidirectional defect dipoles or films, composites, and heterostructures with imprinted fields. As proof of concept, we compare our findings to *ab-initio*-based simulations for the example of unidirectional defect dipoles in $BaTiO_3$. Our simple model can indeed reproduce the qualitative trends and allows for a fundamental understanding of the impact of the field history on the

TABLE I. Optimization strategies of the ECE in the presence of internal bias fields for a fixed field interval $|E_{\text{init}} - E_{\text{end}}|$.

T	Option	ECE	Field interval	Branch	Reversible?
$T < T_0$	1	Inverse	$E_{ex} < E_c^{\text{right}}$	Lower	Yes
	2	Conventional	$E_{ex} > E_c^{\text{left}}$	Upper	Yes
$T' < T < T_0$	5	Conventional	$E_{ex} \leq E_c$	Switching	No
$T \geq T_0$	3	Inverse	$E_{ex} \leq E_d/2$	Lower	Yes
	4	Conventional	$E_{ex} \geq E_d/2$	Upper	Yes

ECE in these systems [22,23]. In the future, more specific models need to be established in order to consider nonhomogeneous internal fields, and the dependency of the internal fields on temperature and possible modifications over time [17]. Our results now have to be confirmed by experiments.

ACKNOWLEDGMENTS

Funding from the Deutsche Forschungsgemeinschaft (DFG) SPP 1599 B3 (Grants No. XU 121/1-2 and No. AL 578/16-2) and A11/B2 (Grant No. GR 4792/1-2) is acknowledged. Additionally, we are grateful to the Lichtenberg-High Performance Computer at TU Darmstadt and the Center for Computational Science and Simulation (CCSS) at University of Duisburg-Essen for the use of their computational resources. We thank Dr. C. Ederer of ETH Zürich and Dr. M. Marathe of the Institut de Ciència de Materials de Barcelona for fruitful discussions.

APPENDIX A: THE INFLUENCE OF THE INITIAL FIELD STRENGTH

The various trends discussed for the ECE depend on the relative strength of E_d and ΔE_{ex}. In Sec. III A, we study different ratios by a systematic variation of the internal field strength for $E_{\text{init}} = 0.2$ and $E_{\text{final}} = 0$. In the following, we show that the same trends occur for a fixed internal field strength ($E_d = -0.6$) and a variation of E_{init}.

In Fig. 12, the results for case (ii), $|E_d| < E_{\text{init}}$, are illustrated. Analogous to Fig. 4, we find the conventional ECE for positively poled samples which is reduced at T' and $T \geq T_0$. It should be noted that we use slightly different ratios of both fields (0.6/0.8 here, compared to 0.06/0.2 in Sec. III A). As already discussed in Sec. III A, the reduction of ΔT is more pronounced for a reduced ratio of both field strengths.

In Fig. 13, the results for case (iii), $|E_d| = E_{\text{init}}$, are summarized. Analogous to Fig. 5, the dipolar entropy change is zero for $T > T'$, as field removal results in the switching of the polarization direction with constant $|P|$. For $E = 0.6$, both the irreversible losses and the dipolar entropy change for $T < T'$ are reduced compared to $E = 0.8$.

In Fig. 14, the results for case (iv), $|E_d| > E_{\text{init}}$, are collected. The same temperature profile of the ECE as in Fig. 6 is observed: inverse ECE due to the dipolar entropy for $T' < T < T''$ and $T > T_0$, conventional ECE due to the dipolar entropy for $T < T'$, and the superposition of conventional (due to losses) and inverse (due to dipolar entropy change) ECE for $T'' < T < T_0$.

In Fig. 15, the results for case (v), $|E_d| = 2E_{\text{init}}$, are summarized. Analogous to Fig. 7, a reversible inverse ECE related to the dipolar entropy change can be found for all temperatures. Furthermore, a reversible conventional ECE can be found for $T < T'$.

We note that a higher internal field strength (here, $E_d = -0.6$) results in an increase of the temperature range $T' < T < T_0$, compared with the discussion in Sec. III A. In addition, we find $T'' = 0.175$, 0.413, 0.873, and 1.0 for

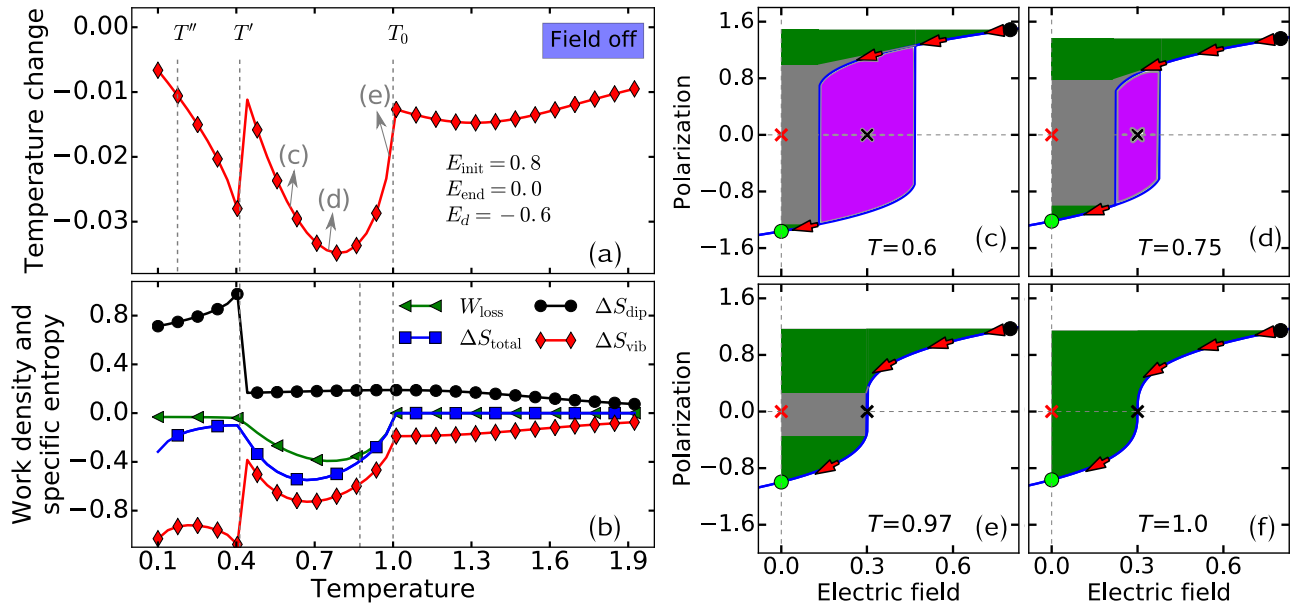

FIG. 12. The electrocaloric effect for $|E_d| < E_{\text{init}}$ in the sample with positively poled initial states, similar to case (ii) in Fig. 4. Black and green dots and black and red crosses mark the initial and final states and the center of hysteresis without and with defects, respectively, and arrows illustrate the direction of the field change.

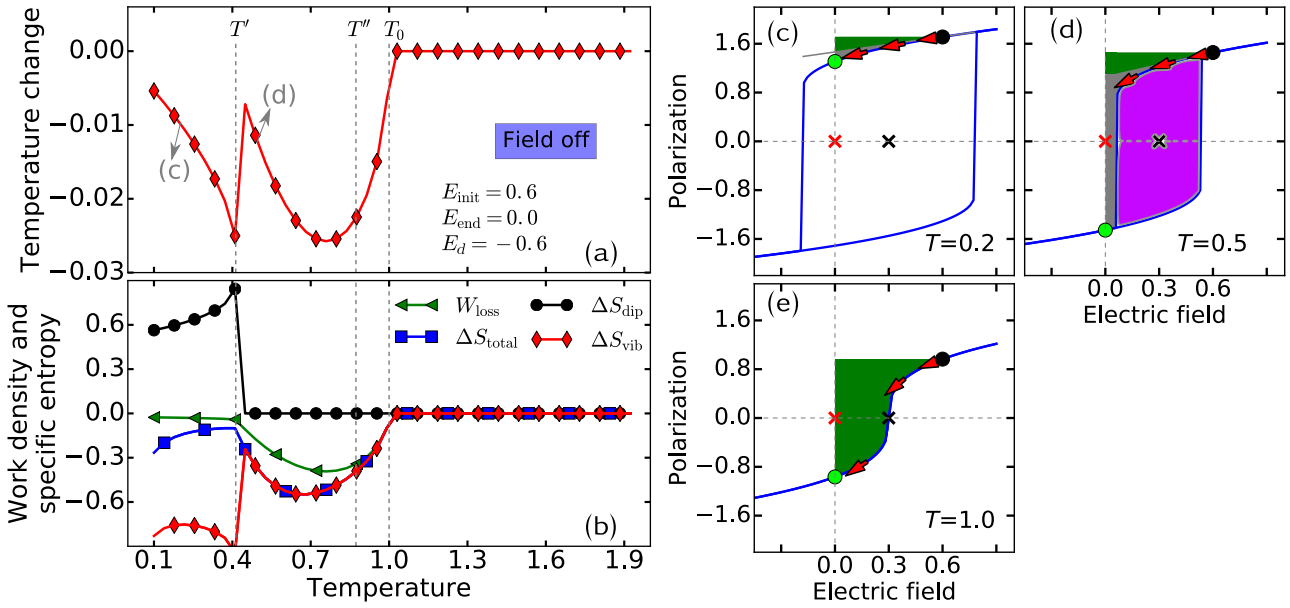

FIG. 13. The electrocaloric effect for $|E_d| = E_{init}$ in the sample with positively poled initial states, similar to case (iii) in Fig. 5. Black and green dots represent the initial and final polarization states, and the arrows describe the direction of the field change. The red and black crosses denote the center of the hysteresis without and with defects, respectively.

$E_{init} = 0.8$, 0.6, 1/3, and 0.3. In other words, T'' increases with a decrease in the ratio $|E_{init}/E_d|$.

In summary, the same tendencies are observed for the similar ratios of E_d and E_{init}, independent of the actual values of the two fields.

APPENDIX B: PARALLEL INTERNAL AND EXTERNAL FIELDS

The main focus of Sec. III is the ECE in the presence of antiparallel internal and external fields. However, as discussed in Sec. III A, shifting the field interval may

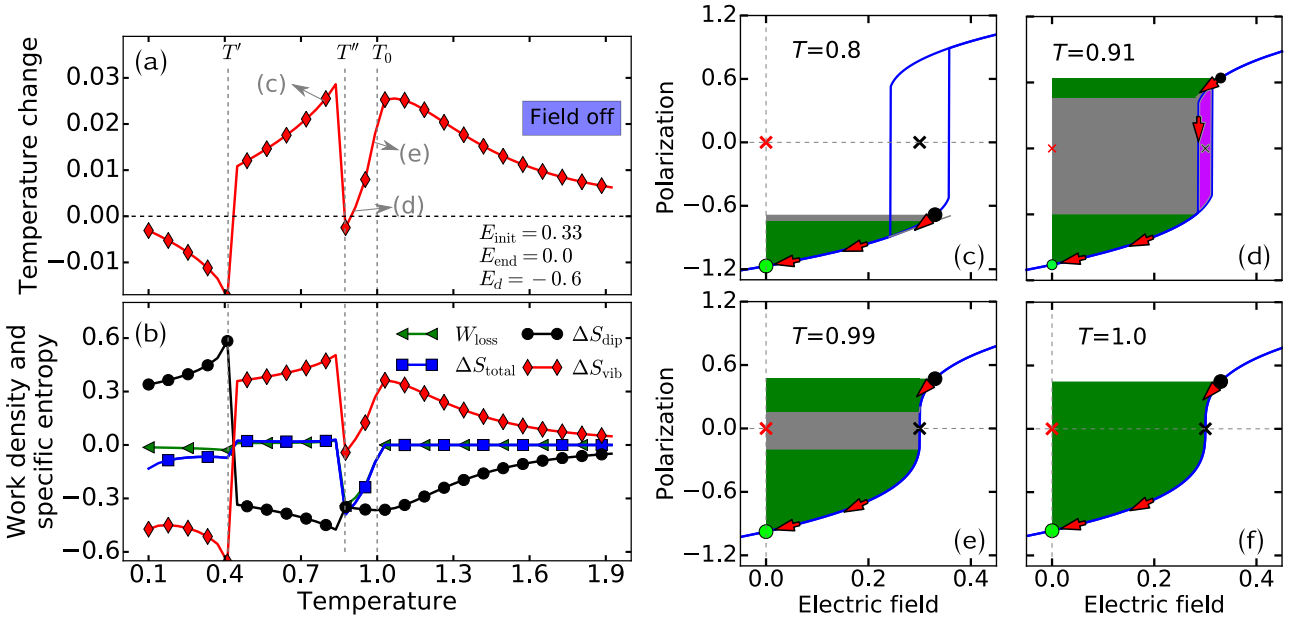

FIG. 14. The electrocaloric effect for $|E_d| > E_{init}$ in the sample with negatively initial poled states for $T' < T < T''$, and positively initial poled states for all other values of T, similar to case (iv) in Fig. 6. Black and green dots represent the initial and final polarization states, and the arrows describe the direction of the field change. The red and black crosses denote the center of the hysteresis without and with defects, respectively.

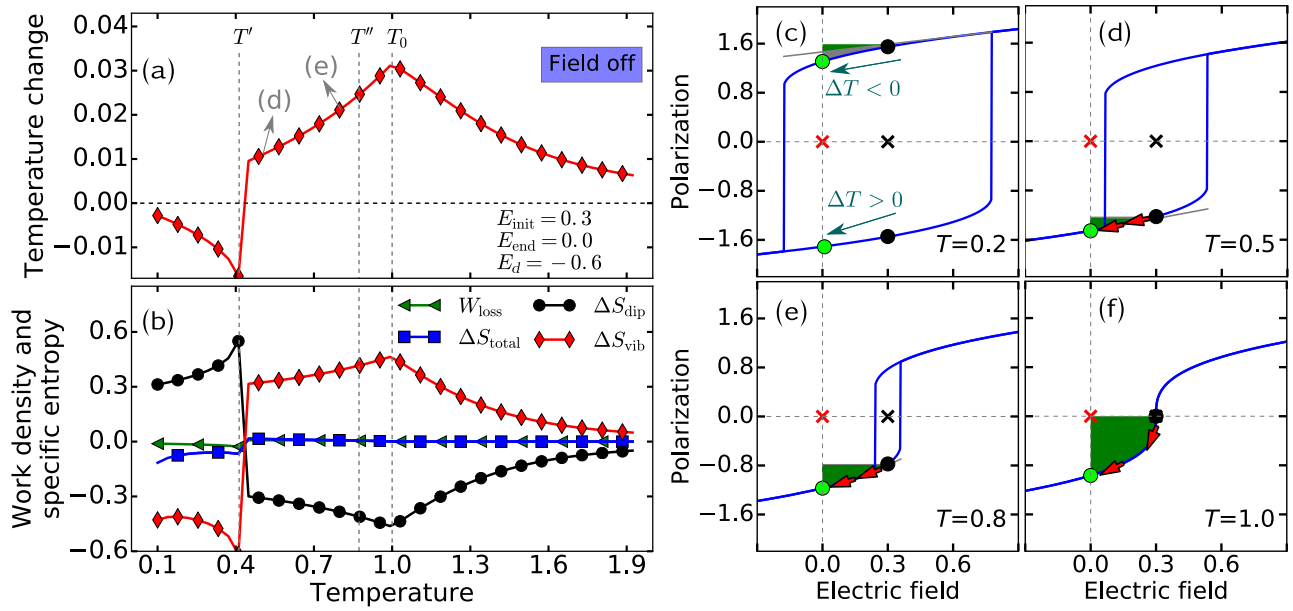

FIG. 15. The electrocaloric effect for $|E_d| = 2E_{\rm init}$ in the sample with negatively initial poled states, similar to case (v) in Fig. 7. Black and green dots and black and red crosses mark the initial and final states and the center of hysteresis without and with defects, respectively, and the arrows illustrate the direction of the field change.

considerably modify the response. In the following, we therefore discuss the impact of parallel internal and external fields for $E_{\rm init} - E_{\rm end} = 0.2$. Thereby, we focus on two cases: $E_d = 0.15 < E_{\rm init}$ and $E_d = 0.3 > E_{\rm init}$.

In the presence of positive bias fields, the left coercive field is always negative and thus no characteristic temperature T' can be defined. In addition, T'' is systematically reduced from 0.55 (no internal fields) to 0.45 and 0.35 for $E_{\rm d} = 0.15$ and 0.3, respectively. In principle, the reversible inverse ECE for a negatively poled sample on the lower branch of hysteresis also occurs, which will not be discussed in the following.

For positively poled samples, we find a reversible conventional ECE, i.e., almost equal cooling for field removal and heating for field application. As shown in Fig. 16, with increasing strength of the internal fields, the ΔT peak position shifts to higher temperatures and broadens. Thus, ΔT above T_0 can be enhanced by the parallel internal fields, whereas the ECE for lower temperatures is slightly reduced.

These findings are in qualitative agreement with the results for parallel internal fields induced by unidirectional defect dipoles, which are randomly distributed in samples [22,23]. In those works, it has been shown that internal bias fields stabilize the ferroelectric phase and systematically shift the ΔT peak to higher T with an increasing internal field strength. Furthermore, the fact that the internal fields may exceed the critical field strength of the first-order paraelectric-to-ferroelectric transition, resulting in a continuous transition, has been discussed.

Analogous to the discussion in Sec. III B, the reversible conventional caloric cooling can be optimized by design option 2, i.e., if the field interval is shifted to the left shoulder of the hysteresis [cf., Figs. 17(b) and 17(c)]. Here, it should be noted that this shoulder point depends on the temperature and the internal field strength. With increasing strength of the internal field, the optimal field interval is thus systematically shifted to negative fields.

Similar to the discussion for negative internal fields, shifting the field interval to the left coercive field for a positively poled sample would further enhance the dipolar entropy change. However, as illustrated in Fig. 17(d),

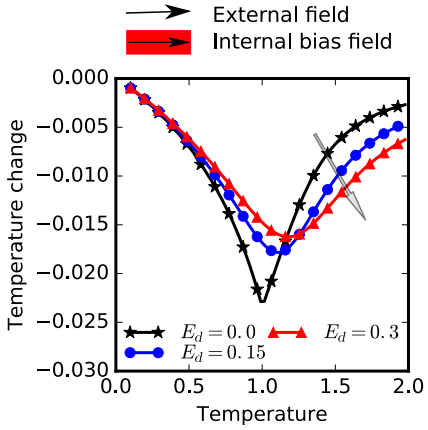

FIG. 16. The influence of parallel internal and external fields on the ECE for $E_{\rm init} = 0.2$ and $E_{\rm final} = 0$ in a positively poled sample.

the switching of the polarization direction is related to large positive work losses and thus results in an irreversible heating of the material for the negative left coercive field. Thus, design option 5 is not applicable for positively poled samples and parallel internal fields. Furthermore, an optimized inverse ECE would be possible for the field interval on the left side of the right coercive field ($E_{ex} < E_c^{\text{right}}$), indicated by the white arrow in Fig. 17(d), using a strategy similar to design option 5.

In summary, parallel internal and external fields favor the conventional ECE and the same optimization strategies as discussed for negative internal fields can be applied.

APPENDIX C: THE INTERNAL FIELD RELATED TO DEFECT DIPOLES—A COMPARISON WITH MOLECULAR-DYNAMICS SIMULATIONS

In the following, we compare the results based on our simple analytical model with uniform bias fields to results based on MD simulations on $BaTiO_3$ with local unidirectional defect dipoles, which are randomly distributed in the sample.

For this purpose, we utilize the effective Hamiltonian approach [57]. This approach is based on a low-order expansion of the energy in terms of the local ferroelectric polarization $\boldsymbol{u}$ and the local strain $\boldsymbol{w}$:

$$\begin{aligned} H^{\text{eff}} = {} & \frac{M^*_{\text{dipole}}}{2}\sum_{\boldsymbol{R},\alpha}\dot{u}^2_\alpha(\boldsymbol{R}) + \frac{M^*_{\text{acoustic}}}{2}\sum_{\boldsymbol{R},\alpha}\dot{w}^2_\alpha(\boldsymbol{R}) \\ & + V^{\text{self}}(\{\boldsymbol{u}\}) + V^{\text{dpl}}(\{\boldsymbol{u}\}) + V^{\text{short}}(\{\boldsymbol{u}\}) \\ & + V^{\text{elas, homo}}(\eta_1,\ldots,\eta_6) + V^{\text{elas, inho}}(\{\boldsymbol{w}\}) \\ & + V^{\text{coup, homo}}(\{\boldsymbol{u}\},\eta_1,\ldots,\eta_6) + V^{\text{coup, inho}}(\{\boldsymbol{u}\},\{\boldsymbol{w}\}), \end{aligned} \tag{C1}$$

where $\eta_1,\ldots,\eta_6$ are the six components of homogeneous strain in Voigt notation. $V^{\text{self}}(\{\boldsymbol{u}\})$ is the self energy of the local mode, $V^{\text{dpl}}(\{\boldsymbol{u}\})$ is the long-range dipole-dipole interaction, $V^{\text{short}}(\{\boldsymbol{u}\})$ is the short-range interaction between local soft modes, $V^{\text{elas, homo}}(\eta_1,\ldots,\eta_6)$ is the elastic energy from homogeneous strain, $V^{\text{elas, inho}}(\{\boldsymbol{w}\})$ is the elastic energy from inhomogeneous strain, $V^{\text{coup, homo}}(\{\boldsymbol{u}\},\eta_1,\ldots,\eta_6)$ is the coupling between the local soft modes and the homogeneous strain, and $V^{\text{coup, inho}}(\{\boldsymbol{u}\},\{\boldsymbol{w}\})$ is the coupling between the soft modes and the inhomogeneous strain. The parametrization used has been constructed for $BaTiO_3$ employing density functional theory [58] and has been successfully applied to predict ferroelectric and electrocaloric properties [7,22]. We use MD simulations to explicitly evolve the three components of the local polarization vector in time, as implemented in the FERAM code [52].

We focus on internal bias fields induced by randomly distributed and perfectly unidirectional defect dipoles.

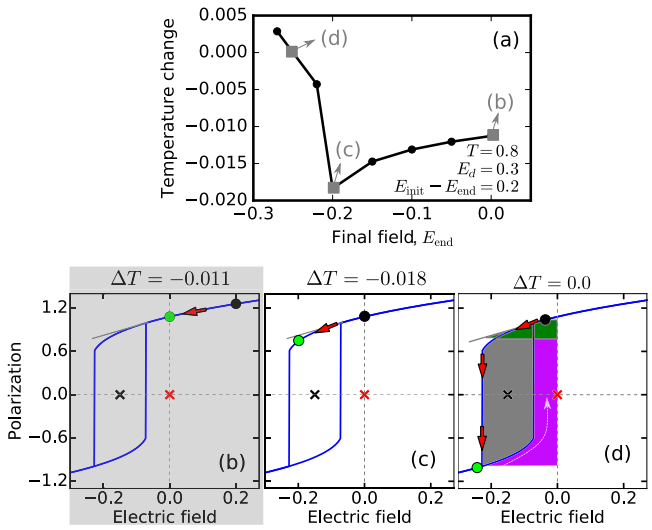

FIG. 17. Tailoring strategies of the ECE through modifying the field protocol. Black and green dots represent the initial and final polarization states, and the arrows describe the direction of the field change. The red and black crosses denote the center of the hysteresis without and with defects, respectively.

Therefore, we fix the local polarization in 1% of the $96 \times 96 \times 96$ $BaTiO_3$ cells in our simulation at -0.5 Cm^{-2} (for further details, see Ref. [22]). In order to determine the ECE, we use the simulation protocol from Ref. [43]. First, we equilibrate the system (180 ps) within an external field of 50 kV/mm along [001] at the given temperature, utilizing a Nosé-Poincaré thermostat [59]. Second, the system evolves in time under adiabatic conditions using the leapfrog method and the change of temperature and polarization are recorded while the field is ramped at a rate of 0.001 (kV/cm)/fs. The coarse graining of the degrees of freedom reduces the specific heat. Thus the model quantitatively overestimates the adiabatic temperature change ΔT. Following Ref. [42], we correct the leading error in ΔT by the rescaling of ΔT with the number of degrees of freedom. Further details on the method and technical aspects can be found in Refs. [22,43].

In agreement with our analytical model, the center of the ferroelectric hysteresis is systematically shifted to positive fields with an increasing strength of the internal field (given by the density or strength of the antiparallel defect dipoles). Furthermore, the hysteresis is systematically reduced with increasing temperature and vanishes in the paraelectric phase.

Induced changes of ferroelectric polarization and the resulting caloric responses for $E_{\text{init}} > E_{\text{final}}$ and a positively poled initial state are illustrated in Fig. 18 for three examples: (1) $T < T_0$ in defect-free material in Figs. 18(a) and 18(b); (2) $T' < T < T_0$ in the presence of antiparallel internal bias fields in Figs. 18(c) and 18(d); and (3) $T > T_0$ in the presence of antiparallel internal bias fields in Figs. 18(e) and 18(f). As discussed in Sec. III B, the

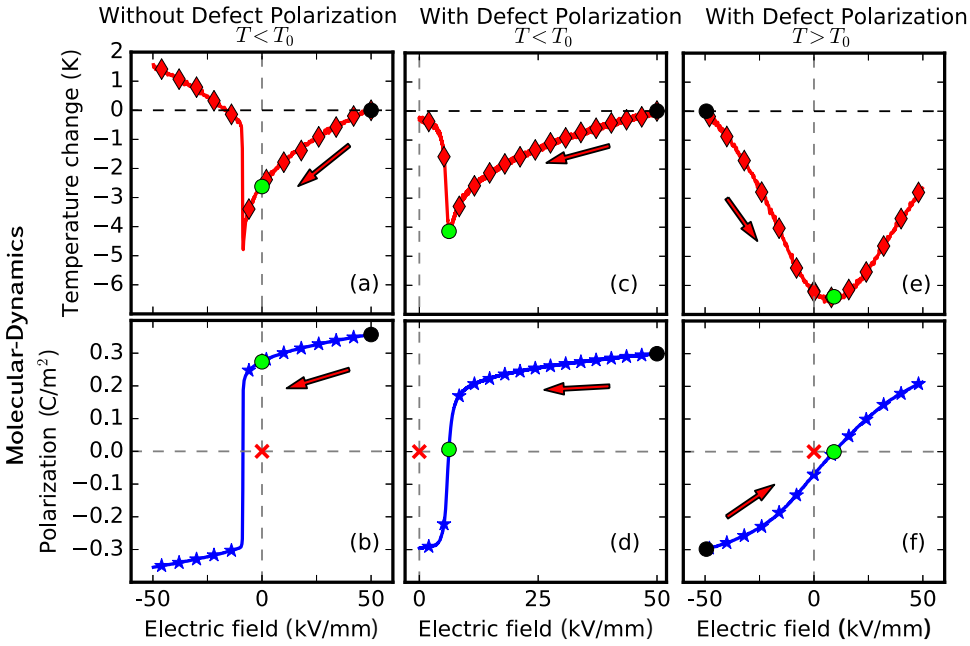

FIG. 18. The change of temperature (a),(c),(e) and polarization (b),(d),(f) as found in *ab-initio*-based MD simulations: (a),(b) below T_0 without defects; (c),(d) below T_0 with antiparallel defects; (e),(f) above T_0 with antiparallel defects. The black dots represent the initial field, and the red arrows indicate the direction of the loading. The centers for defect-free samples are marked as red crosses.

caloric cooling can be optimized by design option 2 when ramping to the shoulder of the hysteresis [see the defect-free sample in Figs. 18(a) and 18(b)], and by design option 4 ($T > T_0$) through ramping to the coercive field [see the samples in the presence of defect dipoles in Figs. 18(e) and 18(f)].

For $T < T_0$ and a negative E_c^{left} [see Figs. 18(a)–18(b)], further shifting of the field interval to the left, beyond the shoulder of the hysteresis, suppresses the positive polarization, and the system heats up due to the work losses, as discussed in Sec. III B. With a further increase of the negative field, the (negative) polarization increases, giving rise to work losses, and suppressing the change of the specific dipolar entropy. Hence, the material heats up further.

Figs. 18(c) and 18(d) summarize the results for defects antiparallel to the positively poled polarization and $T' < T < T_0$. In this case, the switching of the polarization direction from positive to negative takes place at $E_c^{\text{left}} > 0$. The reduction of ΔP in combination with the irreversible negative work loss results in the maximal cooling point being only slightly above the zero polarization point (design option 5). This agrees with the observations in Fig. 10(f). In short, a complex temperature dependency of the inverse ECE on previous poling and the relative strengths of the internal and external fields occurs [22,23]. Furthermore, we note that the simulations also yield a reversible inverse ECE for a strong internal field and $T > T_0$.

In summary, our simple analytical model reproduces the qualitative trends found by means of *ab-initio*-based simulations. In particular, the main trends observed for bias fields induced by local defect dipoles can be modeled by the assumed homogeneous bias field.

[1] J. F. Scott, Applications of modern ferroelectrics, Science (80-.) **315**, 954 (2007).

[2] X. Moya, S. Kar-Narayan, and N. D. Mathur, Caloric materials near ferroic phase transitions, Nat. Mater. **13**, 439 (2014).

[3] J. Wang, T. Yang, K. Wei, and X. Yao, Temperature–electric field hysteresis loop of electrocaloric effect in ferroelectricity—direct measurement and analysis of electrocaloric effect. I, Appl. Phys. Lett. **102**, 152907 (2013).

[4] S. Uddin, G.-P. Zheng, Y. Iqbal, R. Ubic, and J. Yang, Unification of the negative electrocaloric effect in $Bi_{1/2}Na_{1/2}TiO_3$-$BaTiO_3$ solid solutions by $Ba_{1/2}Sr_{1/2}TiO_3$ doping, J. Appl. Phys. **114**, 213519 (2013).

[5] A.-K. Axelsson, F. L. Goupil, L. J. Dunne, G. Manos, M. Valant, and N. M. Alford, Microscopic interpretation of sign reversal in the electrocaloric effect in a ferroelectric $PbMg_{1/3}Nb_{2/3}O_3$-$30PbTiO_3$ single crystal, Appl. Phys. Lett. **102**, 102902 (2013).

[6] P. D. Thacher, Electrocaloric effects in some ferroelectric and antiferroelectric $Pb(Zr,Ti)O_3$ compounds, J. Appl. Phys. **39**, 1996 (1968).

[7] M. Marathe, D. Renggli, M. Sanlialp, M. O. Karabasov, V. V. Shvartsman, D. C. Lupascu, A. Grünebohm, and C. Ederer, Electrocaloric effect in $BaTiO_3$ at all three ferroelectric transitions: Anisotropy and inverse caloric effects, Phys. Rev. B **96**, 014102 (2017).

[8] H. H. Wu and R. E. Cohen, Polarization rotation and the electrocaloric effect in barium titanate, J. Phys. Condens. Matter **29**, 485704 (2017).

[9] Y. Qi, S. Liu, A. M. Lindenberg, and A. M. Rappe, Ultrafast Electric Field Pulse Control of Giant Temperature Change in Ferroelectrics, Phys. Rev. Lett. **120**, 055901 (2018).

[10] Z. Kutnjak, B. Rožič, and R. Pirc, *Wiley Encyclopedia of Electrical and Electronics Engineering* (John Wiley & Sons Inc., Hoboken, New Jersey, USA, 2015).

[11] Yang Liu, James F. Scott, and Brahim Dkhil, Direct and indirect measurements on electrocaloric effect: Recent developments and perspectives, Appl. Phys. Rev. **3**, 031102 (2016).

[12] A. Grünebohm, Y.-B. Ma, M. Marathe, B.-X. Xu, K. Albe, C. Kalcher, K.-C. Meyer, V. V. Shvartsman, D. C. Lupascu, and C. Ederer, On the origins of the inverse electrocaloric effect, Energy Technol. **6**, 1491 (2018).

[13] G. H. Jonker and P. V. Lambeck, Origin of the electrooptical effect in pyroelectric crystals, Ferroelectrics **21**, 641 (1978).

[14] L. Zhang, E. Erdem, X. Ren, and R.-A. Eichel, Reorientation of $(Mn''_{Ti}\text{-}V^{\bullet\bullet}_{O})^{\times}$ defect dipoles in acceptor-modified $BaTiO_3$ single crystals: An electron paramagnetic resonance study, Appl. Phys. Lett. **93**, 202901 (2008).

[15] C. M. Folkman, S. H. Baek, C. T. Nelson, H. W. Jang, T. Tybell, X. Q. Pan, and C. B. Eom, Study of defect-dipoles in an epitaxial ferroelectric thin film, Appl. Phys. Lett. **96**, 052903 (2010).

[16] X. Ren, Large electric-field-induced strain in ferroelectric crystals by point-defect-mediated reversible domain switching, Nat. Mater. **3**, 91 (2004).

[17] P. Erhart, P. Träskelin, and K. Albe, Formation and switching of defect dipoles in acceptor-doped lead titanate: A kinetic model based on first-principles calculations, Phys. Rev. B **88**, 024107 (2013).

[18] Y. A. Genenko, J. Glaum, M. J. Hoffmann, and K. Albe, Mechanisms of aging and fatigue in ferroelectrics, Mater. Sci. Eng. B Ser. Electr. Fatigue **192**, 52 (2015).

[19] H.-S. Han, J. Koruza, E. A. Patterson, J. Schulthei, E. Erdem, W. Jo, J.-S. Lee, and J. Rödel, Hardening behavior and highly enhanced mechanical quality factor in $(K_{0.5}Na_{0.5})NbO_3$-based ceramics, J. Eur. Ceram. Soc. **37**, 2083 (2017).

[20] J. B. J. Chapman, R. E. Cohen, A. V. Kimmel, and D. M. Duffy, Improving the Functional Control of Aged Ferroelectrics Using Insights from Atomistic Modeling, Phys. Rev. Lett. **119**, 177602 (2017).

[21] Z. Xu, Z. Fan, X. Liu, and X. Tan, Impact of phase transition sequence on the electrocaloric effect in $Pb(Nb,Zr,Sn,Ti)O_3$ ceramics, Appl. Phys. Lett. **110**, 082901 (2017).

[22] A. Grünebohm and T. Nishimatsu, Influence of defects on ferroelectric and electrocaloric properties of $BaTiO_3$, Phys. Rev. B **93**, 134101 (2016).

[23] Y.-B. Ma, A. Grünebohm, K.-C. Meyer, K. Albe, and B.-X. Xu, Positive and negative electrocaloric effect in $BaTiO_3$ in the presence of defect dipoles, Phys. Rev. B **94**, 094113 (2016).

[24] X. Qian, H.-J. Ye, T. Yang, W.-Z. Shao, L. Zhen, E. Furman, L.-Q. Chen, and Q.-M. Zhang, Internal biasing in relaxor ferroelectric polymer to enhance the electrocaloric effect, Adv. Funct. Mater. **25**, 5134 (2015).

[25] X. Qian, T. Yang, T. Zhang, L.-Q. Chen, and Q.-M. Zhang, Anomalous negative electrocaloric effect in a relaxor/normal ferroelectric polymer blend with controlled nano- and meso-dipolar couplings, Appl. Phys. Lett. **108**, 142902 (2016).

[26] D. Lee, B. C. Jeon, A. Yoon, Y. J. Shin, M. H. Lee, T. K. Song, S. D. Bu, M. Kim, J.-S. Chung, J.-G. Yoon, and T. W. Noh, Flexoelectric control of defect formation in ferroelectric epitaxial thin films, Adv. Mater. **26**, 5005 (2014).

[27] Y.-H. Chu, Q. He, C.-H. Yang, P. Yu, L. W. Martin, P. Shafer, and R. Ramesh, Nanoscale control of domain architectures in $BiFeO_3$ thin films, Nano Lett. **9**, 1726 (2009).

[28] Y. Zhou, H. K. Chan, C. H. Lam, and F. G. Shin, Mechanisms of imprint effect on ferroelectric thin films, J. Appl. Phys. **98**, 024111 (2005).

[29] M. T. Kesim, M. W. Cole, J. Zhang, I. B. Misirlioglu, and S. P. Alpay, Tailoring dielectric properties of ferroelectric-dielectric multilayers, Appl. Phys. Lett. **104**, 022901 (2014).

[30] M. T. Kesim, J. Zhang, S. P. Alpay, and L. W. Martin, Enhanced electrocaloric and pyroelectric response from ferroelectric multilayers, Appl. Phys. Lett. **105**, 52901 (2014).

[31] G. Akcay, S. P. Alpay, G. A. Rossetti, Jr., and J. F. Scott, Influence of mechanical boundary conditions on the electrocaloric properties of ferroelectric thin films, J. Appl. Phys. **103**, 024104 (2008).

[32] L. J. Dunne, M. Valant, A.-K. Axelsson, G. Manos, and N. M. Alford, Statistical mechanical lattice model of the dual-peak electrocaloric effect in ferroelectric relaxors and the role of pressure, J. Phys. D: Appl. Phys. **44**, 375404 (2011).

[33] J. Mangeri, K. C. Pitike, S. P. Alpay, and S. Nakhmanson, Amplitudon and phason modes of electrocaloric energy interconversion, npj Comput. Mater. **2**, 16020 (2016).

[34] M. C. Rose and R. E. Cohen, Giant Electrocaloric Effect Around T_C, Phys. Rev. Lett. **109**, 187604 (2012).

[35] S. Bin-Omran, I. A. Kornev, and L. Bellaiche, Wang-Landau Monte Carlo formalism applied to ferroelectrics, Phys. Rev. B **93**, 014104 (2016).

[36] Y. Liu, J. F. Scott, and B. Dkhil, Some strategies for improving caloric responses with ferroelectrics, APL Mater. **4**, 64109 (2016).

[37] Y.-B. Ma, N. Novak, K. Albe, and B.-X. Xu, Optimized electrocaloric effect by field reversal: Analytical model, Appl. Phys. Lett. **109**, 202906 (2016).

[38] J. Wang, T. Yang, S. Chen, G. Li, and X. Yao, Characteristics and dielectric properties of $(Pb_{0.97-x}La_{0.02}Ba_x)(Zr_{0.72}Sn_{0.22}Ti_{0.06})O_3$ ceramics, J. Alloys Compd. **539**, 280 (2012).

[39] N. Novak, Z. Kutnjak, and R. Pirc, High-resolution electrocaloric and heat capacity measurements in barium titanate, EPL **103**, 47001 (2013).

[40] Y. Bai, K. Ding, G.-P. Zheng, S.-Q. Shi, and L. Qiao, Entropy-change measurement of electrocaloric effect of $BaTiO_3$ single crystal, Phys. Status Solidi A **209**, 941 (2012).

[41] I. Ponomareva and S. Lisenkov, Bridging the Macroscopic and Atomistic Descriptions of the Electrocaloric Effect, Phys. Rev. Lett. **108**, 167604 (2012).

[42] T. Nishimatsu, J. A. Barr, and S. P. Beckman, Direct molecular dynamics simulation of electrocaloric effect in $BaTiO_3$, J. Phys. Soc. Jpn. **82**, 114605 (2013).

[43] M. Marathe, A. Grünebohm, T. Nishimatsu, P. Entel, and C. Ederer, First-principles-based calculation of the

electrocaloric effect in $BaTiO_3$: A comparison of direct and indirect methods, Phys. Rev. B **93**, 054110 (2016).

[44] Y.-B. Ma, K. Albe, and B.-X. Xu, Lattice-based Monte Carlo simulations of the electrocaloric effect in ferroelectrics and relaxor ferroelectrics, Phys. Rev. B **91**, 184108 (2015).

[45] Y.-B. Ma, N. Novak, J. Koruza, T. Yang, K. Albe, and B.-X. Xu, Enhanced electrocaloric cooling in ferroelectric single crystals by electric field reversal, Phys. Rev. B **94**, 100104(R) (2016).

[46] Y.-B. Ma, C. Molin, V. V. Shvartsman, S. Gebhardt, D. C. Lupascu, K. Albe, and B.-X. Xu, State transition and electrocaloric effect of $BaZr_xTi_{1-x}O_3$: Simulation and experiment, J. Appl.Phys. **121**, 024103 (2017).

[47] M. Marathe, C. Ederer, and A. Grünebohm, The impact of hysteresis on the electrocaloric effect at first-order phase transitions, Phys. Status Solidi Basic Res. **255**, 1700308 (2018).

[48] X. Moya, E. Stern-Taulats, S. Crossley, D. González-Alonso, S. Kar-Narayan, A. Planes, L. Mañosa, and N. D. Mathur, Giant electrocaloric strength in single-crystal $BaTiO_3$, Adv. Mater. **25**, 1360 (2013).

[49] Y. Bai, X. Han, and L. Qiao, Optimized electrocaloric refrigeration capacity in lead-free $(1-x)BaZr_{0.2}Ti_{0.8}O_3$-$xBa_{0.7}Ca_{0.3}TiO_3$ ceramics, Appl. Phys. Lett. **102**, 252904 (2013).

[50] V. Basso, J.-F. Gerard, and S. Pruvost, Doubling the electrocaloric cooling of poled ferroelectric materials by bipolar cycling, Appl. Phys. Lett. **105**, 52907 (2014).

[51] R. Pirc, Z. Kutnjak, R. Blinc, and Q.-M. Zhang, Electrocaloric effect in relaxor ferroelectrics, J. Appl. Phys. **110**, 74113 (2011).

[52] T. Nishimatsu, U. V. Waghmare, Y. Kawazoe, and D. Vanderbilt, Fast molecular-dynamics simulation for ferroelectric thin-film capacitors using a first-principles effective Hamiltonian, Phys. Rev. B **78**, 104104 (2008).

[53] D. Bolten, U. Böttger, T. Schneller, M. Grossmann, O. Lohse, and R. Waser, Reversible and irreversible processes in doner-doped $Pb(Zr,Ti)O_3$, Appl. Phys. Lett. **77**, 3830 (2000).

[54] D. Bolten, U. Böttger, and R. Waser, Frequency and temperature dependence of the relative permittivity in ferroelectrics: Monte-Carlo simulation study, J. Appl. Phys. **93**, 2890 (2003).

[55] We note that the temperature dependency of c_{ph} in the temperature range of interest is negligible apart from phase transitions.

[56] We note that $\Delta S_{\mathrm{total}}$ scales with $1/T$. Therefore, tiny work losses already result in a finite change of the total entropy for very low temperatures.

[57] W. Zhong, D. Vanderbilt, and K. M. Rabe, First-principles theory of ferroelectric phase transitions for perovskites: The case of $BaTiO_3$, Phys. Rev. B **52**, 6301 (1995).

[58] Takeshi Nishimatsu, Masaya Iwamoto, Yoshiyuki Kawazoe, and Umesh V. Waghmare, First-principles accurate total energy surfaces for polar structural distortions of $BaTiO_3$, $PbTiO_3$ and $SrTiO_3$: Consequences for structural transition temperatures, Phys. Rev. B **82**, 134106 (2010).

[59] S. D. Bond, B. J. Leimkuhler, and B. B. Laird, The Nosé-Poincaré method for constant temperature molecular dynamics, J. Comput. Phys. **151**, 114 (1999).